

Vapour pressure deficit is the main driver of tree canopy conductance across biomes

Victor Flo¹, Jordi Martínez-Vilalta¹, Víctor Granda¹, Maurizio Mencuccini¹, and Rafael Poyatos¹

¹CREAF

November 30, 2022

Abstract

We aim to identify the relative importance of vapour pressure deficit (VPD), soil water content (SWC) and photosynthetic photon flux density (PPFD) as drivers of tree canopy conductance, which is a key source of uncertainty for modelling vegetation responses under climate change. We use sap flow time series of 1858 trees in 122 sites from the SAPFLUXNET global database to obtain whole-tree canopy conductance (G). The coupling, defined as the percentage of variance (R²) of G explained by the three main hydrometeorological drivers (VPD, SWC and PPFD), was evaluated using linear mixed models. For each hydrometeorological driver we assess differences in coupling among biomes, and use multiple linear regression to explain R² by climate, soil and vegetation structure. We found that in most areas tree canopy conductance is better explained by VPD than by SWC or PPFD. We also found that sites in drylands are less coupled to all three hydrometeorological drivers than those in other biomes. Climate, soil and vegetation structure were common controls of all three hydrometeorological couplings with G, with wetter climates, fine textured soils and tall vegetation being associated to tighter coupling. Differences across sites in the hydrometeorological coupling of tree canopy conductance may affect predictions of ecosystem dynamics under future climates, and should be accounted for explicitly in models.

1 **Vapour pressure deficit is the main driver of tree canopy conductance across biomes**

2 Víctor Flo¹, Jordi Martínez-Vilalta^{1,2}, Víctor Granda¹, Maurizio Mencuccini^{1,3}, Rafael
3 Poyatos^{1,2}

4 ¹CREAF, E08193 Bellaterra (Cerdanyola del Vallès), Catalonia, Spain

5 ²Univ Autònoma de Barcelona, Cerdanyola del Vallès 08193, Spain

6 ³ICREA, Barcelona 08010, Spain

7 ***Corresponding author: Víctor Flo (v.flo@creaf.uab.cat)**

8 **VF:** 0000-0003-1908-4577

9 **JMV:** 0000-0002-2332-7298

10 **VG:** 0000-0002-0469-1991

11 **MM:** 0000-0003-0840-1477

12 **RP:** 0000-0003-0521-2523

13

14 **Key points**

- 15
- Vapour pressure deficit is the main driver of tree canopy conductance globally.
 - Tree canopy conductance dynamics are poorly explained by the main hydrometeorological drivers in drylands.
 - Tree canopy conductance is more tightly coupled to hydrometeorological drivers in wetter sites, fine textured soils and tall vegetation.
- 16
- 17
- 18
- 19

20 **Abstract**

21 We aim to identify the relative importance of vapour pressure deficit (VPD), soil water
22 content (SWC) and photosynthetic photon flux density (PPFD) as drivers of tree canopy
23 conductance, which is a key source of uncertainty for modelling vegetation responses under
24 climate change. We use sap flow time series of 1858 trees in 122 sites from the
25 SAPFLUXNET global database to obtain whole-tree canopy conductance (G). The
26 coupling, defined as the percentage of variance (R^2) of G explained by the three main
27 hydrometeorological drivers (VPD, SWC and PPF), was evaluated using linear mixed
28 models. For each hydrometeorological driver we assess differences in coupling among
29 biomes, and use multiple linear regression to explain R^2 by climate, soil and vegetation
30 structure. We found that in most areas tree canopy conductance is better explained by VPD
31 than by SWC or PPF. We also found that sites in drylands are less coupled to all three
32 hydrometeorological drivers than those in other biomes. Climate, soil and vegetation
33 structure were common controls of all three hydrometeorological couplings with G , with
34 wetter climates, fine textured soils and tall vegetation being associated to tighter coupling.
35 Differences across sites in the hydrometeorological coupling of tree canopy conductance
36 may affect predictions of ecosystem dynamics under future climates, and should be
37 accounted for explicitly in models.

38

39 **Keywords**

40 biome, global, radiation, sap flow, soil water content, transpiration

41 **1. Introduction**

42 Plants regulate transpiration in response to variation in hydrometeorological conditions.
43 However, despite decades of ecophysiological research measuring responses of leaf, plant
44 or ecosystem evaporative fluxes to atmospheric dryness, soil moisture and radiation
45 (Beerling, 2015), the relative importance of these drivers in determining plant controls on
46 transpiration at the global scale is still poorly known. It is important to disentangle the
47 biogeographical patterns of the individual dominant drivers of transpiration control, as such
48 drivers are expected to show spatially heterogeneous dynamics with global change (Zhou *et*
49 *al.*, 2019). Thus, understanding their separate roles may help improve models to anticipate
50 climate change impacts on vegetation function and on global water and carbon cycles, and
51 to disentangle land-atmosphere feedbacks (Massmann *et al.*, 2019).

52

53 Conductance to water vapour (G) derived from leaf, plant or ecosystem evaporative fluxes
54 has been frequently used to describe the dynamic control of transpiration by plants at
55 different organisational and temporal scales (Jarvis & McNaughton, 1986). At short
56 timescales, this regulation is carried out via changes in stomatal aperture. Under low soil
57 water content (SWC) or high atmospheric water demand, which is often assessed using
58 atmospheric vapour pressure deficit (VPD), plants reduce G to avoid dangerous declines in
59 water potentials preventing physiological damage and severe dehydration (Oren *et al.*,
60 1999). In contrast, G responses to light (i.e. photosynthetic photon flux density, PPFD) are
61 linked to plant water use efficiency (WUE). Thus, plants would increase G with PPFD in
62 order to optimize photosynthesis in relation to water loss (Sperry *et al.*, 2016). In addition,
63 PPFD effects on G may be driven by the need to regulate leaf temperature under high

64 radiation levels (Fauset *et al.*, 2018). These responses have been assessed in multiple, single-
65 site studies (Jarvis, 1976; Oren *et al.*, 1999; Wang *et al.*, 2020). However, the fact that these
66 studies frequently used different phenomenological models and model-fitting approaches
67 complicates synthesis efforts aimed at building a common understanding of the dynamics
68 of G at broad spatial scales. In addition, most previous work focused on overall G
69 sensitivity (e.g. Hoshika *et al.*, 2018), not on the importance of the individual drivers (but
70 see for instance Bretfeld *et al.*, 2018), hampering our understanding of which
71 hydrometeorological drivers dominate G regulation globally.

72

73 Large-scale syntheses of the relative importance of hydrometeorological drivers regulating
74 transpiration have been conducted using ecosystem evapotranspiration data. Novick *et al.*
75 (2016) compared the limiting effect of SWC and VPD across vegetation types and climates,
76 and found that limitation on ecosystem surface conductance to water vapour caused by
77 SWC increased with climatic dryness, but that VPD was higher than SWC limitation across
78 most mesic biomes. Similarly, Han *et al.* (2020) also reported an increased importance of
79 SWC with increasing ecosystem aridity, but instead found that net radiation was more
80 relevant than VPD. Conversely, Zhao *et al.* (2019) identified that, globally, ecosystem
81 evapotranspiration was not primarily limited by hydrometeorological drivers, but by
82 vegetation height, followed by SWC and PPFD. However, these results may not reflect the
83 relative importance of hydrometeorological drivers on tree transpiration regulation, since
84 partitioning transpiration from total evapotranspiration can be problematic and show
85 substantial variability across ecosystems (Berkelhammer *et al.*, 2016). Here, we overcome

86 the limitations of ecosystem-scale approaches by taking advantage of the first global
87 database of plant-level transpiration from sap flow measurements (Poyatos *et al.*, 2021).

88

89 In this study, we investigate the hydrometeorological coupling of tree-level canopy
90 conductance by quantifying the explanatory power (R^2) of individual hydrometeorological
91 drivers of G (VPD, SWC, PPF). We also estimate the total predictive ability of a model
92 including all three drivers. We then examine how the hydrometeorological coupling of G
93 differs across biomes as a function of climate, soil properties and vegetation structure. We
94 hypothesize differences in absolute and relative G coupling to the hydrometeorological
95 drivers across biomes as a result of specific environmental constraints, with tighter
96 coupling with VPD and SWC in drier biomes with higher exposure to drought stress. We
97 also expect that climate, soil and vegetation structure determine the coupling of G with
98 VPD, SWC and PPF, with greater coupling in sites experiencing drier conditions and
99 marked climatic seasonality, in fine textured soils associated with lower soil water
100 availability, and in tall stands with low leaf areas that are expected to have tighter coupling
101 to G due to thinner canopy boundary layers (Peng *et al.*, 2019).

102

103 **2. Methods**

104 *2.1. Sapflow and environmental data*

105 We extracted 1858 time series of tree sap flow from the SAPFLUXNET database (Poyatos
106 *et al.*, 2021). These time series met our requirements for data quality (see filtering section
107 below), did not include any experimental treatment (Table S1) and corresponded to 130
108 species on 122 sites (Table S2). Sub-daily sap flow time series were obtained directly in

109 sap flux density units (SFD; [$\text{cm}^3 \text{ cm}^{-2}_{\text{Asw}} \text{ h}^{-1}$]) or, when sapwood area was not available, in
110 whole-tree sap flow units (SF; [$\text{cm}^3 \text{ h}^{-1}$]; 24 out of 122 data-sets). In those latter cases, SF
111 time series were converted to SFD units by dividing SF data by an estimation of tree
112 sapwood area (A_{sw}) using a global allometric relationship as a function of tree basal area
113 and functional type (i.e. angiosperm vs gymnosperm) as predictors ($R^2 = 0.78$; $n = 2262$)
114 (Fig. S1). Sub-daily SFD time series were aggregated to daytime SFD values (i.e., 6 am to
115 6 pm solar time). Following Flo *et al.* (2019), sap flow time series measured with non-
116 calibrated heat dissipation sensors were corrected for bias in absolute SFD multiplying by a
117 constant factor (1.405).

118

119 Similarly to SFD, we obtained VPD [kPa] and PPFD [$\mu\text{mol m}^{-2} \text{ s}^{-1}$] time series for each
120 site from SAPFLUXNET on-site measurements, which were subsequently averaged to
121 daytime values. When PPFD data were not available in the datasets (12 out of 122 sites),
122 PPFD was calculated using the mean short-wave radiation between 6 am and 6 pm
123 extracted from the ERA5 re-analyses data base (Copernicus Climate Change Service (C3S),
124 2017) and then multiplying by 2.3 to transform it into PPFD. Soil water content (SWC; v/v)
125 data were missing in 43% of the SAPFLUXNET datasets included in this study. To ensure
126 homogeneity across sites, we used SWC from the 15-30 cm soil depth layer obtained from
127 the ERA5-land reanalysis dataset (Copernicus Climate Change Service (C3S), 2019) at 9x9
128 km resolution (see database validation in Flo *et al.*, 2021).

129

130 *2.2. Data filtering*

131 In order to minimize seasonal phenological changes in leaf area, we excluded all periods
 132 between 15 days before the first daytime average temperature under 0°C and 30 days after
 133 the last day with temperatures under 0°C, during the cold season of each site (similar to
 134 Novick *et al.*, 2016). To prevent artefacts in whole-tree canopy conductance calculation
 135 (Ewers & Oren, 2000), we filtered out rainy days –days when SWC increased– and days
 136 when average daytime VPD was under 0.3 kPa (Anderegg *et al.*, 2018). We also ensured a
 137 sufficient range in hydrometeorological conditions by discarding sites with a total VPD
 138 range below 0.5 kPa or SWC range below 0.05 m³ m⁻³, and with PPF maximum values
 139 below 400 μmol m⁻²_{Asw} s⁻¹.

140

141 2.3. Whole-tree canopy conductance calculation

142 To obtain G_s , we firstly transformed SFD units from [cm³ cm⁻²_{Asw} h⁻¹] to [Kg m⁻²_{Asw} s⁻¹] and
 143 then we converted it to daytime tree canopy conductance per unit of sapwood area G_{Asw}
 144 [mol m⁻²_{Asw} s⁻¹] following Phillips & Oren (1998) and a unit transformation (eq.1).

$$145 \quad G_{Asw,j,i,k} = \frac{(115.8 + 0.4236 T_{j,i}) SFD_{j,i,k}}{VPD_{j,i}} \eta \frac{T_0}{(T_0 + T_{j,i})} e^{-0.00012h_i} \quad (1)$$

146 Where $SFD_{j,i,k}$ is the sap flux density value of each site (j), day (i), and tree (k); $T_{j,i}$ [°C] is
 147 the temperature, $VPD_{j,i}$ [kPa] is the daytime vapour pressure deficit, η equals 44.6 mol m⁻³,
 148 T_0 is 273 K, and h [m] is the altitude of each site. For two sites where h values were not
 149 available, it was extracted from The Shuttle Radar Topography Mission (Earth Resources
 150 Observation And Science (EROS) Center, 2017).

151

152 2.4. Hydrometeorological coupling quantification

153 We define hydrometeorological coupling as the coefficient of determination (R^2) of simple
154 and multiple linear mixed models of VPD, SWC and PPFD explaining G_{Asw} at the site-tree
155 level. High R^2 levels imply high predictive power of hydrometeorological drivers over G_{Asw} .
156 We fitted uni-variate models for each site using G_{Asw} as response variable and the neperian
157 logarithm of each driver as predictor (Fig. S2). Similarly, we also fitted additive, multiple
158 regression models of site-level G_{Asw} as a function of the logarithm of all three
159 hydrometeorological drivers (FULL model). The hierarchical structure of species and trees
160 within sites was taken into account using linear mixed models, implemented with the *lmer*
161 function of the ‘lme4’ R package (Bates *et al.*, 2015). When sites had more than one tree
162 per species and more than one species (54 out of 122 sites), random intercept and slopes
163 parameters were fitted for species, and random intercept parameters for trees nested into
164 species. When models did not converge, the random structure was simplified and only the
165 random intercept for trees was considered (33 out of 54 sites). When sites had just one
166 species and multiple trees (67 out of 122 sites), we fitted a random intercept for trees. When
167 a site had multiple species and just one tree per species (1 out of 122), random intercept and
168 slopes were fitted for species.

169

170 Since we were interested in the overall coupling of all the individuals at a site,
171 hydrometeorological coupling was set as the conditional R^2 of the models (i.e. R^2_{VPD} , R^2_{SWC} ,
172 R^2_{PPFD} , R^2_{FULL}) (Table S3), calculated with the ‘MuMIn’ R package (Bartoń, 2020). We
173 fitted simple and multiple regression models instead of more sophisticated non-linear
174 models to reduce complexity and gain generalizability across the data sets.

175

176 Three alternative sets of models were fitted to ensure consistency of the estimated R^2_{VPD} ,
177 R^2_{SWC} , R^2_{PPFD} and R^2_{FULL} values (Fig. S3). Firstly, we checked for issues related to
178 unbalanced distributions of G_{Asw} throughout the range of VPD, SWC or PPFD. To do that,
179 we repeated the same models as above but using binned data (binned data models).
180 Specifically, we calculated the average of G_{Asw} measurements comprised in 0.2 kPa VPD
181 intervals, five site-specific SWC intervals and 250 $\mu\text{mol m}^{-2}_{Asw} \text{s}^{-1}$ PPFD intervals. For each
182 summarized G_{Asw} we defined a specific VPD, SWC and PPFD value as the average of the
183 data inside each bin. Secondly, to avoid possible artefacts due to the different sample size at
184 each site, models were repeated by randomly sampling 10 days per tree. We implemented a
185 bootstrapping approach with 100 repetitions and coupling values were calculated as the
186 median of the R^2 's distributions of each model (sampled data models). Finally, the third
187 alternative implied obtaining coupling estimates by means of more flexible generalized
188 additive models (GAM), as implemented in the bam function of the 'mgcv' R package
189 (Wood, 2011). These GAM models were fitted using all the data available per site and
190 specifying the same random structure as the simple linear models described above. The
191 alternative R^2 's coupling metrics obtained with the binned data, the sampled data and the
192 gam models were all very similar to the R^2 's coupling metrics from the linear models using
193 all data (Fig. S3), and hence the latter were used in all the following analyses.

194

195 *2.5. Biome classification and plot-level bioclimatic data*

196 The estimates of G_{Asw} hydrometeorological coupling were complemented with site-level
197 data on climate, soil properties and vegetation structure. These data were either directly
198 obtained from the metadata associated to each SAPFLUXNET dataset or from additional
199 data sources. We took from SAPFLUXNET the biome corresponding to each site –obtained

200 from Whittaker diagrams using Chelsa Climate databases (Karger *et al.*, 2017) (Fig. S4)–
201 and carried out an exhaustive quality control to reassign site biomes as indicated by
202 SAPFLUXNET datasets contributors (Table S2). Biomes were simplified into 5 groups;
203 drylands (DRY), woodlands (WOOD), temperate forest (TEMP), boreal forests (BOR) and
204 tropical forests (TROP) (Table S3 and Fig. S4).

205

206 For each site, we extracted climate information from global rasters (Fig. S5). We used
207 monthly mean precipitation, monthly maximum temperature and monthly minimum
208 temperature rasters for the period 1979 to 2013 from the Chelsa Climate databases (Karger
209 *et al.*, 2017), to estimate monthly potential evapotranspiration (mPET), annual potential
210 evapotranspiration (PET) and mean annual precipitation (MAP) using the ‘envirem’ R
211 package (Title & Bemmels, 2018). Then, we calculated MAP over PET (PPET) as a water
212 availability index, and the standard deviation of the monthly differences between mean
213 precipitation and mPET (P-PETsd) as an index of seasonality in water availability.
214 Relevant soil parameters were obtained from in situ SAPFLUXNET data and
215 complemented with SoilGrids 2.0 (Hengl *et al.*, 2017) when data were not available in
216 SAPFLUXNET (Table S4). We used the proportion of sand and clay particles in the fine
217 earth fraction [%], the total nitrogen [g kg^{-1}] and the depth to bedrock (up to 200 cm) to
218 characterize soils. We used bedrock depth because of its ecological relevance, but results
219 for this variable should be considered with caution due to its particularly high variability at
220 fine spatial scales. Stand height was available in SAPFLUXNET for most sites. When this
221 was not the case, information was completed using the average tree height of the
222 corresponding site (again from SAPFLUXNET, 3 out of 122 sites) or when both were

223 absent it was extracted from the Global 1 km Forest Canopy Height raster (Simard *et al.*,
224 2011) (3 out of 122 sites) (Table S4). When site LAI was not available from
225 SAPFLUXNET (37 out of 122 sites), it was estimated as the average of the 95th percentile
226 of the period 2010 to 2016 of the MCD15A3H.006 MODIS Leaf Area Index product
227 (0.5x0.5 km grid) (Myneni, 2015), calculated using Google Earth Engine (Gorelick *et al.*,
228 2017) (Table S4).

229

230 2.6. Statistical Analyses

231 In order to test whether the hydrometeorological coupling of G_{Asw} varies across biomes, we
232 fitted weighted regressions using the modelled R^2_{VPD} , R^2_{SWC} , R^2_{PPFD} and R^2_{FULL} as response
233 variables and biome as explanatory variable (fixed factor). The number of tree-days with
234 SFD measurements in each site was used as a weighting variable. Similarly, we also tested
235 the significance of cross-biome differences between paired hydrometeorological couplings
236 (e.g. difference between VPD and SWC coupling, $R^2_{VPD} - R^2_{SWC}$) using the same model
237 structure.

238

239 We further explained the biogeographical patterns in the hydrometeorological coupling
240 across sites as a function of climate, soil properties and vegetation structure. We fitted four
241 multiple weighted regression models with R^2_{VPD} , R^2_{SWC} , R^2_{PPFD} and R^2_{FULL} as response
242 variables and $\log(\text{PPET})$, $\log(\text{P-PETsd})$, soil % clay, soil total nitrogen, soil bedrock depth,
243 stand height and LAI as bioclimatic predictors (Fig. S5). We also used the number of tree-
244 days of each site as weighting variable. Sand percentage was not included due to a high
245 correlation with soil % clay ($r = -0.73$). A stepwise model selection process based on

246 minimising AIC was applied. We checked for normality and homoscedasticity of residuals
247 in all models, and we also checked for multicollinearity by quantifying Variance Inflation
248 Factors (VIF) using the ‘performance’ R package (Lüdtke *et al.*, 2020). These models were
249 combined with the rasters of bioclimatic data (at a uniform resolution of 9x9 km), to predict
250 and map global patterns of G hydrometeorological coupling to VPD, SWC and PPFD.

251

252 We also assessed the relative importance of each hydrometeorological driver by extracting
253 the marginal partial R^2 of each hydrometeorological variable in the FULL model. These
254 partial R^2 were calculated using ‘r2beta’ function of the R ‘r2glmm’ package (Jaeger, 2017)
255 and relativized by the sum of the three partial R^2 (relative R^2). These relative R^2 values can
256 be interpreted as the relative importance of each hydrometeorological variable in explaining
257 daily variations in canopy conductance. Then, similarly as above, we fitted three multiple
258 weighted regression models using the estimated relative R^2 as response variables and the
259 bioclimatic variables as predictors. The resulting models were used to project the relative
260 importance of each hydrometeorological driver globally. All statistical analyses were
261 performed in R 4.0.5 (R Core Team, 2021).

262

263 **3. Results**

264 We found large differences in the coupling of G_{Asw} (R^2 coupling metric) to each of the
265 individual hydrometeorological drivers globally and among biomes (Fig. 1 and Table 1).
266 We observed that G_{Asw} was predominantly coupled to VPD across biomes, whereas
267 coupling to SWC and PPFD was comparatively less important (Fig. 1). The difference
268 between the coupling to VPD and to the other two drivers was significant in all cases

269 except for SWC on woodlands and for both SWC and PPF_D in boreal biomes (Table 1).
270 The coupling to SWC was higher for TEMP and particularly WOOD biomes whereas
271 PPF_D tended to dominate in TROP biome (marginally significant effect) (Table 1). The
272 outcomes of the linear models show a significantly higher VPD and SWC coupling for
273 TEMP, TROP and also WOOD biomes than for the DRY biome (Table. 1). The PPF_D
274 coupling was also lowest for the DRY biome and was significantly higher for TEMP, BOR
275 and TROP biomes; the G_{Asw} coupling to PPF_D was also significantly lower in the WOOD
276 biome compared to TEMP and TROP biomes (Table 1). The DRY biome was the one in
277 which all three drivers collectively (FULL model) explained less variability in G_{Asw} .

278

279 In the models explaining the biogeographical patterns of G_{Asw} hydrometeorological
280 coupling (which explained 30-52% of the variance), soil and vegetation structure variables
281 were identified as common controls on the G_{Asw} hydrometeorological coupling (Table 2). In
282 particular, soil clay %, and stand height were selected for all three hydrometeorological
283 drivers (i.e. VPD, SWC and PPF_D) and the FULL model, with tighter coupling always
284 associated to fine textured soils and taller vegetation. In addition, higher soil nitrogen
285 concentrations had a positive effect on VPD, PPF_D and overall (FULL model) coupling.
286 Log(PPET) and bedrock depth were only selected for the R^2_{SWC} and the FULL models, in
287 which lower climatic water availability and deeper soils were associated with looser
288 coupling (Table 2). Higher LAI was associated with lower VPD, SWC and overall (FULL
289 model) coupling, although the effect was only significant for the FULL model. Seasonality
290 in water availability (P-PETsd) was not included in any of the models.

291

292 When predictions of G_{Asw} coupling to each of the hydrometeorological drivers were mapped
293 at the global scale, spatial patterns differed substantially among drivers (Fig. 2). G_{Asw}
294 coupling to VPD was higher than ca. 50% almost everywhere except for some sub-tropical
295 regions. The regulation of tree water fluxes at high northern latitudes (above 50° N) and in
296 tropical regions was highly coupled to VPD, SWC and PPFD (Fig. 2). In contrast, trees
297 living in subtropical regions tended to be less coupled (Fig. 2), consistent with the lower
298 coupling to individual drivers in WOOD and particularly DRY biomes (Table 1). When
299 considering the relative importance (partial R^2) of each of the three variables in driving
300 canopy conductance (Fig. 3), temperate regions, drylands and savannas were typically
301 coupled to VPD, many boreal areas were coupled to PPFD, and tropical regions tended to
302 be coupled to both VPD and PPFD (Fig. 3). Although a relevant role of SWC in
303 conjunction with VPD was identified in some regions (e.g. SW Asia, Mediterranean basin),
304 SWC did not consistently emerge as a regionally important, dominant predictor of G_{Asw} .

305

306 **4. Discussion**

307 This study provides the first examination of the importance of VPD, SWC and PPFD as the
308 main hydrometeorological drivers of tree canopy conductance (G) at the global level. All
309 sites presented some degree of coupling to the hydrometeorological drivers considered,
310 although there was substantial variability in the magnitude of this coupling (i.e. R^2_{VPD} ,
311 R^2_{SWC} , R^2_{PPFD}). We demonstrate that G is predominantly coupled to VPD in most biomes,
312 while G regulation caused by SWC and PPFD is generally comparably lower.

313

314 Our results clearly identify vapour pressure deficit as the major regulator of G globally.
315 This is consistent with recent reports showing that VPD limits vegetation growth at the

316 global scale (Babst *et al.*, 2019; Yuan *et al.*, 2019), but contradicts other studies focusing on
317 the controls of primary productivity (Jung *et al.*, 2017; Liu *et al.*, 2020) that find a global
318 dominant role of SWC. However, caution is needed when comparing our results with these
319 remote sensing and ecosystem-level studies, as our sample size is much smaller (and
320 possibly spatially biased), and our approach focuses at the plant-level and uses actual
321 transpiration data. In addition, we consider the effect of radiation availability, which has
322 been rarely assessed in this type of studies.

323

324 We did not observe the hypothesized increase in coupling to VPD and SWC in drier
325 biomes, although, as expected, coupling to VPD and SWC was tighter than coupling to
326 PPF_D in temperate and particularly woodland biomes. Interestingly, the importance of
327 SWC decreased in DRY biome, even if actual sensitivity to SWC was high (Fig. S2). This
328 result contrasts to those found at the ecosystem level, showing that drier sites present larger
329 SWC control over evapotranspiration than wetter ones (Novick *et al.*, 2016). This opposite
330 result between transpiration and evapotranspiration drivers importance suggests that the
331 bare soil and the understory contribution to ecosystem surface conductance may be large
332 (Li *et al.*, 2019) and strongly driven by SWC in DRY biome (Scott *et al.*, 2021).

333

334 The low coupling of G to all three hydrometeorological drivers in drylands is intriguing and
335 may be related to the diversity of water use strategies in water limited systems, which range
336 from drought-deciduousness to deep rooting or high hydraulic safety (e.g. Ackerly, 2004;
337 Jacobsen *et al.*, 2007). Deep roots reaching the groundwater, for instance, could allow
338 sufficient water supply to uncouple transpiration from hydrometeorological drivers and

339 specifically from shallow SWC (Barbeta & Peñuelas, 2017). At the other extreme, exposure
340 to low water potentials results in early stomatal closure (Martin-StPaul *et al.*, 2017),
341 effectively disconnecting transpiration from hydrometeorological drivers for long periods
342 of the year. Memory effects (Ogle *et al.*, 2015) are also likely to be more common in water-
343 limited systems, which may result in more complex responses of transpiration to individual
344 hydrometeorological drivers. In addition, in water-limited regions SWC can show strong
345 seasonal interactions with VPD (Zhou *et al.*, 2019) and PPFD (Boese *et al.*, 2019) (see also
346 Figs. S6-S8), which could produce compound drought effects that would complicate
347 disentangling the coupling of transpiration to individual drivers. Finally, it should also be
348 noted that we focus here on relatively tall woody vegetation, as this is the one likely to be
349 measured with sap flow sensors (Poyatos *et al.*, 2021), and hence our analysis excludes
350 extremely arid sites likely to be totally driven by water availability (compare the grey areas
351 in our Fig. 3 with Fig. 1 in Running *et al.* (2004)).

352 Beyond general biome effects, differences in coupling among sites were explained by
353 differences in soil, stand structure, and to a lesser extent by climate. Besides the lower
354 coupling with SWC in areas with less climatic water availability, consistent with the results
355 discussed in the previous paragraph, our results show the key importance of soil
356 characteristics, particularly texture, in explaining variability in *G* coupling. Trees increase
357 the coupling to all three hydrometeorological drivers under high clay content (finer
358 texture). This result is to be expected since plants in fine textured soils would effectively
359 experience lower water potentials more gradually as SWC decreases, than plants in more
360 coarsely textured soils that will experience a threshold-like transition from high to low
361 water potentials (Hillel, 1998). Hence, sandy soils dry rapidly and trees end up spending a

362 large fraction of their time at very low soil water potential, reducing the coupling. In
363 addition, our results indicate that deeper soils (higher bedrock depth) were associated to
364 lower coupling to SWC, consistent with the notion that access to deep water may uncouple
365 transpiration from shallow SWC (Barbeta & Peñuelas, 2017).

366

367 Vegetation height and LAI are also important drivers of vegetation transpiration coupling.
368 VPD, SWC and PPFD limitations to G were typically higher in taller trees, consistent with
369 previous studies (Boese *et al.*, 2019; Zhao *et al.*, 2019). Tree height is associated with
370 productive areas with high resource availability, including water. In general, taller trees
371 have higher water transport efficiencies and lower resistance to embolism (Liu *et al.*, 2019;
372 Flo *et al.*, 2021). These traits are associated with acquisitive water use strategies and a tighter
373 stomatal control of transpiration (Klein, 2014). A similar argument can be used to explain
374 tighter coupling to VPD and radiation in areas with high soil nitrogen concentrations, as the
375 latter have been related to increased stomatal conductance (Maire *et al.*, 2015) and greater
376 degree of stomatal control under drought (Ewers *et al.*, 1999). Taller canopies are also more
377 aerodynamically rough and, therefore, show higher VPD coupling due to higher levels of
378 leaf surface VPD. Interestingly, once accounting for the effect of vegetation height LAI had
379 a negative effect on transpiration coupling to VPD. We associate this result to the fact that
380 higher LAI is related to lush canopy structures that would have a significant proportion of
381 the leaves effectively decoupled from the atmosphere (Zhang *et al.*, 2016).

382

383 Differences in coupling among sites should also reflect different water use strategies in the
384 corresponding communities. These differences are reflected in part in the climatic, soil, and

385 structural differences we studied. However, independently of coupling strength, these
386 relationships had a relatively large proportion of unexplained variance, which could be
387 related to contrasting water use strategies coexisting in the same biomes and even in the
388 same sites (Anderegg *et al.*, 2018; Denham *et al.*, 2021). This implies that species traits should
389 be accounted for if we aim to understand the fine-scale distribution of G responses (Flo *et*
390 *al.*, 2021) and predict ecosystem-level responses to environmental variation.

391

392 In conclusion, we found that VPD is the main hydrometeorological driver of tree canopy
393 conductance globally but we also showed that VPD coupling did not increase in warmer
394 sites, as found in ecosystem-level studies (Novick *et al.*, 2016). The role of VPD in driving
395 transpiration regulation will likely be larger in a warmer world, given the generalised
396 increases in projected VPD (Grossiord *et al.*, 2020). Our results indicate clear differences in
397 hydrometeorological couplings among biomes and under different environmental contexts,
398 which likely underlie observed differences in the dynamics of vegetation water use, tree
399 growth and ecosystem production. Importantly, the low hydrometeorological coupling
400 observed in drylands suggests that models simulating vegetation-atmosphere fluxes may
401 fail in these regions unless additional processes are considered (Pan *et al.*, 2020). An explicit
402 consideration of plant water transport (Anderegg & Venturas, 2020) and of differences in
403 plant water use strategies (Flo *et al.*, 2021) appear essential to characterize and model the
404 effects of VPD, SWC and PPFD on tree water use and their variability in space and time.

405

406

407

408 **Acknowledgements**

409 This work was supported by the Spanish Ministry of Education, Culture and Sports,
410 through a doctoral grant (FPU15/03939) awarded to VF and by the Spanish Ministry of
411 Science and Innovation through grants CGL2014-55883-JIN and RTI2018-095297-J-I00.
412 RP also acknowledges support by an Alexander von Humboldt Fellowship for Experienced
413 Researchers. JM-V benefited from an ICREA Academia award.

414

415 **Data availability statement**

416 The data that support the findings of this study are openly available at Flo, V. (2021).
417 Vapour pressure deficit is the main driver of tree canopy conductance across biomes (4.0)
418 [Data set]. Zenodo. <https://doi.org/10.5281/zenodo.5517725>

419 The code used to obtain the results of the study can be found at
420 https://github.com/vflo/drivers_importance

421

422 **5. References**

Ackerly, D. (2004) Functional strategies of chaparral shrubs in relation to seasonal water deficit and disturbance. *Ecological Monographs*, **74**, 25–44.

Anderegg, W.R.L., Konings, A.G., Trugman, A.T., Yu, K., Bowling, D.R., Gabbitas, R., Karp, D.S., Pacala, S., Sperry, J.S., Sulman, B.N. & Zenes, N. (2018) Hydraulic diversity of forests regulates ecosystem resilience during drought. *Nature*, **561**, 538–541.

Anderegg, W.R.L. & Venturas, M.D. (2020) Plant hydraulics play a critical role in Earth system fluxes. *New Phytologist*, **226**, 1535–1538.

- Babst, F., Bouriaud, O., Poulter, B., Trouet, V., Girardin, M.P. & Frank, D.C. (2019) Twentieth century redistribution in climatic drivers of global tree growth. *Science Advances*, **5**, eaat4313.
- Barbeta, A. & Peñuelas, J. (2017) Relative contribution of groundwater to plant transpiration estimated with stable isotopes. *Scientific Reports*, **7**, 10580.
- Bartoń, K. (2020) MuMIn: Multi-Model Inference. *R package version 1.43.17*.
- Bates, D., Mächler, M., Bolker, B. & Walker, S. (2015) Fitting Linear Mixed-Effects Models Using **lme4**. *Journal of Statistical Software*, **67**.
- Beerling, D.J. (2015) Gas valves, forests and global change: a commentary on Jarvis (1976) ‘The interpretation of the variations in leaf water potential and stomatal conductance found in canopies in the field.’ *Philosophical Transactions of the Royal Society B: Biological Sciences*, **370**, 20140311.
- Berkelhammer, M., Noone, D.C., Wong, T.E., Burns, S.P., Knowles, J.F., Kaushik, A., Blanken, P.D. & Williams, M.W. (2016) Convergent approaches to determine an ecosystem’s transpiration fraction. *Global Biogeochemical Cycles*, **30**, 933–951.
- Boese, S., Jung, M., Carvalhais, N., Teuling, A.J. & Reichstein, M. (2019) Carbon–Water Flux Coupling Under Progressive Drought. *Biogeosciences*, **16**, 2557–2572.
- Bretfeld, M., Ewers, B.E. & Hall, J.S. (2018) Plant water use responses along secondary forest succession during the 2015-2016 El Niño drought in Panama. *New Phytologist*, **219**, 885–899.
- Copernicus Climate Change Service (C3S) (2019) C3S ERA5-Land reanalysis. *Copernicus Climate Change Service*, May 2020.
- Copernicus Climate Change Service (C3S) (2017) ERA5: Fifth generation of ECMWF atmospheric reanalyses of the global climate. *Copernicus Climate Change Service Climate Data Store (CDS)*, May 2020.

Denham, S.O., Oishi, A.C., Miniati, C.F., Wood, J.D., Yi, K., Benson, M.C. & Novick, K.A. (2021) Eastern US deciduous tree species respond dissimilarly to declining soil moisture but similarly to rising evaporative demand. *Tree Physiology*, **41**, 944–959.

Earth Resources Observation And Science (EROS) Center (2017) Shuttle Radar Topography Mission (SRTM) 1 Arc-Second Global.

Ewers, B., Oren, I., Albaugh, T.J. & Dougherty, P. (1999) Carry-over effects of water and nutrient supply on water use of *Pinus taeda*. *Ecological Applications*, **9**, 513–525.

Ewers, B.E. & Oren, R. (2000) Analyses of assumptions and errors in the calculation of stomatal conductance from sap flux measurements. *Tree Physiology*, **20**, 579–589.

Fauset, S., Freitas, H.C., Galbraith, D.R., Sullivan, M.J.P., Aidar, M.P.M., Joly, C.A., Phillips, O.L., Vieira, S.A. & Gloor, M.U. (2018) Differences in leaf thermoregulation and water use strategies between three co-occurring Atlantic forest tree species: Leaf energy balance of Atlantic forest trees. *Plant, Cell & Environment*, **41**, 1618–1631.

Flo, V., Martínez-Vilalta, J., Mencuccini, M., Granda, V., Anderegg, W.R.L. & Poyatos, R. (2021) Climate and functional traits jointly mediate tree water-use strategies. *New Phytologist*, **231**, 617–630.

Flo, V., Martinez-Vilalta, J., Steppe, K., Schuldt, B. & Poyatos, R. (2019) A synthesis of bias and uncertainty in sap flow methods. *Agricultural and Forest Meteorology*, **271**, 362–374.

Gorelick, N., Hancher, M., Dixon, M., Ilyushchenko, S., Thau, D. & Moore, R. (2017) Google Earth Engine: Planetary-scale geospatial analysis for everyone. *Remote Sensing of Environment*, **202**, 18–27.

Grossiord, C., Buckley, T.N., Cernusak, L.A., Novick, K.A., Poulter, B., Siegwolf, R.T.W., Sperry, J.S. & McDowell, N.G. (2020) Plant responses to rising vapor pressure deficit. *New Phytologist*, **226**, 1550–1566.

Han, Q., Liu, Q., Wang, T., Wang, L., Di, C., Chen, X., Smettem, K. & Singh, S.K. (2020) Diagnosis of environmental controls on daily actual evapotranspiration across a global flux tower network: the roles of water and energy. *Environmental Research Letters*, **15**, 124070.

Hengl, T., Mendes de Jesus, J., Heuvelink, G.B.M., Ruiperez Gonzalez, M., Kilibarda, M., Blagotić, A., Shangguan, W., Wright, M.N., Geng, X., Bauer-Marschallinger, B., Guevara, M.A., Vargas, R., MacMillan, R.A., Batjes, N.H., Leenaars, J.G.B., Ribeiro, E., Wheeler, I., Mantel, S. & Kempen, B. (2017) SoilGrids250m: Global gridded soil information based on machine learning. *PLOS ONE*, **12**, e0169748.

Hillel, D. (1998) *Environmental soil physics*, Academic Press, San Diego, CA.

Hoshika, Y., Osada, Y., de Marco, A., Peñuelas, J. & Paoletti, E. (2018) Global diurnal and nocturnal parameters of stomatal conductance in woody plants and major crops. *Global Ecology and Biogeography*, **27**, 257–275.

Jacobsen, A.L., Pratt, R.B., Davis, S.D. & Ewers, F.W. (2007) Cavitation resistance and seasonal hydraulics differ among three arid Californian plant communities. *Plant, Cell & Environment*, **30**, 1599–1609.

Jaeger, B. (2017) r2glmm: Computes R Squared for Mixed (Multilevel) Models. *CRAN version 0.1.2*.

Jarvis, P.G. (1976) The interpretation of the variations in leaf water potential and stomatal conductance found in canopies in the field. *Philosophical Transactions of the Royal Society of London. B, Biological Sciences*, **273**, 593–610.

Jarvis, P.G. & McNaughton, K.G. (1986) *Stomatal Control of Transpiration: Scaling Up from Leaf to Region. Advances in Ecological Research*, pp. 1–49. Elsevier.

Jung, M., Reichstein, M., Schwalm, C.R., Huntingford, C., Sitch, S., Ahlström, A., Arneth, A., Camps-Valls, G., Ciais, P., Friedlingstein, P., Gans, F., Ichii, K., Jain, A.K., Kato, E., Papale, D., Poulter, B., Raduly, B., Rödenbeck, C., Tramontana, G., Viovy, N., Wang, Y.-P., Weber, U., Zaehle, S. & Zeng, N. (2017) Compensatory water effects link yearly global land CO₂ sink changes to temperature. *Nature*, **541**, 516–520.

Karger, D.N., Conrad, O., Böhner, J., Kawohl, T., Kreft, H., Soria-Auza, R.W., Zimmermann, N.E., Linder, H.P. & Kessler, M. (2017) Climatologies at high resolution for the earth's land surface areas. *Scientific Data*, **4**, 170122.

Klein, T. (2014) The variability of stomatal sensitivity to leaf water potential across tree species indicates a continuum between isohydric and anisohydric behaviours. *Functional Ecology*, **28**, 1313–1320.

Li, X., Gentine, P., Lin, C., Zhou, S., Sun, Z., Zheng, Y., Liu, J. & Zheng, C. (2019) A simple and objective method to partition evapotranspiration into transpiration and evaporation at eddy-covariance sites. *Agricultural and Forest Meteorology*, **265**, 171–182.

Liu, H., Gleason, S.M., Hao, G., Hua, L., He, P., Goldstein, G. & Ye, Q. (2019) Hydraulic traits are coordinated with maximum plant height at the global scale. *Science Advances*, **5**, eaav1332.

Liu, L., Gudmundsson, L., Hauser, M., Qin, D., Li, S. & Seneviratne, S.I. (2020) Soil moisture dominates dryness stress on ecosystem production globally. *Nature Communications*, **11**, 4892.

Lüdecke, Makowski, Waggoner, & Patil (2020) Assessment of Regression Models Performance. *CRAN*.

Maire, V., Wright, I.J., Prentice, I.C., Batjes, N.H., Bhaskar, R., van Bodegom, P.M., Cornwell, W.K., Ellsworth, D., Niinemets, Ü., Ordonez, A., Reich, P.B. & Santiago, L.S. (2015) Global effects of soil and climate on leaf photosynthetic traits and rates: Effects of soil and climate on photosynthetic traits. *Global Ecology and Biogeography*, **24**, 706–717.

Martin-StPaul, N., Delzon, S. & Cochard, H. (2017) Plant resistance to drought depends on timely stomatal closure. *Ecology Letters*, **20**, 1437–1447.

Massmann, A., Gentine, P. & Lin, C. (2019) When Does Vapor Pressure Deficit Drive or Reduce Evapotranspiration? *Journal of Advances in Modeling Earth Systems*, **11**, 3305–3320.

Myneni, Y.K. (2015) MCD15A3H MODIS/Terra+Aqua Leaf Area Index/FPAR 4-day L4 Global 500m SIN Grid V006. *NASA EOSDIS Land Processes DAAC*, May 2020.

Novick, K.A., Ficklin, D.L., Stoy, P.C., Williams, C.A., Bohrer, G., Oishi, A.C., Papuga, S.A., Blanken, P.D., Noormets, A., Sulman, B.N., Scott, R.L., Wang, L. & Phillips, R.P. (2016) The increasing importance of atmospheric demand for ecosystem water and carbon fluxes. *Nature Climate Change*, **6**, 1023–1027.

Ogle, K., Barber, J.J., Barron-Gafford, G.A., Bentley, L.P., Young, J.M., Huxman, T.E., Loik, M.E. & Tissue, D.T. (2015) Quantifying ecological memory in plant and ecosystem processes. *Ecology Letters*, **18**, 221–235.

Oren, R., Sperry, J.S., Katul, G.G., Pataki, D.E., Ewers, B.E., Phillips, N. & Schäfer, K.V.R. (1999) Survey and synthesis of intra- and interspecific variation in stomatal sensitivity to vapour pressure deficit: Intra- and interspecific variation in stomatal sensitivity to vapour pressure deficit. *Plant, Cell & Environment*, **22**, 1515–1526.

Pan, S., Pan, N., Tian, H., Friedlingstein, P., Sitch, S., Shi, H., Arora, V.K., Haverd, V., Jain, A.K., Kato, E., Lienert, S., Lombardozzi, D., Nabel, J.E.M.S., Ottlé, C., Poulter, B., Zaehle, S. &

Running, S.W. (2020) Evaluation of global terrestrial evapotranspiration using state-of-the-art approaches in remote sensing, machine learning and land surface modeling. *Hydrology and Earth System Sciences*, **24**, 1485–1509.

Peng, L., Zeng, Z., Wei, Z., Chen, A., Wood, E.F. & Sheffield, J. (2019) Determinants of the ratio of actual to potential evapotranspiration. *Global Change Biology*, **25**, 1326–1343.

Phillips, N. & Oren, R. (1998) A comparison of daily representations of canopy conductance based on two conditional time-averaging methods and the dependence of daily conductance on environmental factors. *Annales des Sciences Forestières*, **55**, 217–235.

Poyatos, R., Granda, V., Flo, V., Adams, M.A., Adorján, B., Aguadé, D., Aidar, M.P.M., Allen, S., Alvarado-Barrientos, M.S., Anderson-Teixeira, K.J., Aparecido, L.M., Arain, M.A., Aranda, I., Asbjornsen, H., Baxter, R., Beamesderfer, E., Berry, Z.C., Berveiller, D., Blakely, B., Boggs, J., Bohrer, G., Bolstad, P.V., Bonal, D., Bracho, R., Brito, P., Brodeur, J., Casanoves, F., Chave, J., Chen, H., Cisneros, C., Clark, K., Cremonese, E., Dang, H., David, J.S., David, T.S., Delpierre, N., Desai, A.R., Do, F.C., Dohnal, M., Domec, J.-C., Dzikiti, S., Edgar, C., Eichstaedt, R., El-Madany, T.S., Elbers, J., Eller, C.B., Euskirchen, E.S., Ewers, B., Fonti, P., Forner, A., Forrester, D.I., Freitas, H.C., Galvagno, M., Garcia-Tejera, O., Ghimire, C.P., Gimeno, T.E., Grace, J., Granier, A., Griebel, A., Guangyu, Y., Gush, M.B., Hanson, P.J., Hasselquist, N.J., Heinrich, I., Hernandez-Santana, V., Herrmann, V., Hölttä, T., Holwerda, F., Irvine, J., Isarangkool Na Ayutthaya, S., Jarvis, P.G., Jochheim, H., Joly, C.A., Kaplick, J., Kim, H.S., Klemedtsson, L., Kropp, H., Lagergren, F., Lane, P., Lang, P., Lapenas, A., Lechuga, V., Lee, M., Leuschner, C., Limousin, J.-M., Linares, J.C., Linderson, M.-L., Lindroth, A., Llorens, P., López-Bernal, Á., Loranty, M.M., Lüttschwager, D., Macinnis-Ng, C., Maréchaux, I., Martin, T.A., Matheny, A., McDowell, N., McMahon, S., Meir, P., Mészáros, I., Migliavacca, M., Mitchell, P., Mölder, M., Montagnani, L., Moore, G.W., Nakada, R., Niu, F., Nolan, R.H., Norby, R., Novick, K., Oberhuber, W., Obojes, N., Oishi, A.C., Oliveira, R.S., Oren, R., Ourcival, J.-M., Paljakka, T., Perez-Priego, O., Peri, P.L.,

Peters, R.L., Pfautsch, S., Pockman, W.T., Preisler, Y., Rascher, K., Robinson, G., Rocha, H., Rocheteau, A., Röhl, A., Rosado, B.H.P., Rowland, L., Rubtsov, A.V., Sabaté, S., Salmon, Y., Salomón, R.L., Sánchez-Costa, E., Schäfer, K.V.R., Schuldt, B., Shashkin, A., Stahl, C., Stojanović, M., Suárez, J.C., Sun, G., Szatniewska, J., Tatarinov, F., Tesař, M., Thomas, F.M., Tor-ngern, P., Urban, J., Valladares, F., van der Tol, C., van Meerveld, I., Varlagin, A., Voigt, H., Warren, J., Werner, C., Werner, W., Wieser, G., Wingate, L., Wullschleger, S., Yi, K., Zweifel, R., Steppe, K., Mencuccini, M. & Martínez-Vilalta, J. (2021) Global transpiration data from sap flow measurements: the SAPFLUXNET database. *Earth System Science Data*, **13**, 2607–2649.

R Core Team (2021) *R: A Language and Environment for Statistical Computing*, R Foundation for Statistical Computing, Vienna, Austria.

Running, S.W., Nemani, R.R., Heinsch, F.A., Zhao, M., Reeves, M. & Hashimoto, H. (2004) A Continuous Satellite-Derived Measure of Global Terrestrial Primary Production. *BioScience*, **54**, 547–560.

Schöley, J. & Kashnitsky, I. (2020) tricolore: A Flexible Color Scale for Ternary Compositions.

Scott, R.L., Knowles, J.F., Nelson, J.A., Gentine, P., Li, X., Barron-Gafford, G., Bryant, R. & Biederman, J.A. (2021) Water Availability Impacts on Evapotranspiration Partitioning. *Agricultural and Forest Meteorology*, **297**, 108251.

Simard, M., Pinto, N., Fisher, J.B. & Baccini, A. (2011) Mapping forest canopy height globally with spaceborne lidar. *Journal of Geophysical Research*, **116**, G04021.

Sperry, J.S., Wang, Y., Wolfe, B.T., Mackay, D.S., Anderegg, W.R.L., McDowell, N.G. & Pockman, W.T. (2016) Pragmatic hydraulic theory predicts stomatal responses to climatic water deficits. *New Phytologist*, **212**, 577–589.

Title, P.O. & Bemmels, J.B. (2018) ENVIREM: an expanded set of bioclimatic and topographic variables increases flexibility and improves performance of ecological niche modeling. *Ecography*, **41**, 291–307.

Wang, Y., Sperry, J.S., Anderegg, W.R.L., Venturas, M.D. & Trugman, A.T. (2020) A theoretical and empirical assessment of stomatal optimization modeling. *New Phytologist*, **227**, 311–325.

Wood, S.N. (2011) Fast stable restricted maximum likelihood and marginal likelihood estimation of semiparametric generalized linear models: Estimation of Semiparametric Generalized Linear Models. *Journal of the Royal Statistical Society: Series B (Statistical Methodology)*, **73**, 3–36.

Yuan, W., Zheng, Y., Piao, S., Ciais, P., Lombardozzi, D., Wang, Y., Ryu, Y., Chen, G., Dong, W., Hu, Z., Jain, A.K., Jiang, C., Kato, E., Li, S., Lienert, S., Liu, S., Nabel, J.E.M.S., Qin, Z., Quine, T., Sitch, S., Smith, W.K., Wang, F., Wu, C., Xiao, Z. & Yang, S. (2019) Increased atmospheric vapor pressure deficit reduces global vegetation growth. *Science Advances*, **5**, eaax1396.

Zhang, Z.Z., Zhao, P., McCarthy, H.R., Zhao, X.H., Niu, J.F., Zhu, L.W., Ni, G.Y., Ouyang, L. & Huang, Y.Q. (2016) Influence of the decoupling degree on the estimation of canopy stomatal conductance for two broadleaf tree species. *Agricultural and Forest Meteorology*, **221**, 230–241.

Zhao, W.L., Gentine, P., Reichstein, M., Zhang, Y., Zhou, S., Wen, Y., Lin, C., Li, X. & Qiu, G.Y. (2019) Physics-Constrained Machine Learning of Evapotranspiration. *Geophysical Research Letters*, **46**, 14496–14507.

Zhou, S., Williams, A.P., Berg, A.M., Cook, B.I., Zhang, Y., Hagemann, S., Lorenz, R., Seneviratne, S.I. & Gentine, P. (2019) Land–atmosphere feedbacks exacerbate concurrent soil drought and atmospheric aridity. *Proceedings of the National Academy of Sciences*, **116**, 18848–18853.

423 Table 1. Analysis of variance testing differences among biomes in the coupling (conditional
 424 R^2 's from mixed models) of tree-level water conductance (G_{Asw}) to each of the main
 425 hydrometeorological drivers: vapour pressure deficit (R^2_{VPD}), soil water content (R^2_{SWC}),
 426 radiation (R^2_{PPFD}) and the complete model including all drivers (R^2_{FULL}). The table shows the
 427 mean coupling obtained across all sites in each biome. We also show the means of the
 428 paired differences between individual hydrometeorological couplings and the
 429 corresponding statistical significance. DRY: dry and desert biomes; WOOD: woodlands
 430 and shrublands; TEMP: temperate biomes; BOR: boreal and tundra; TROP: tropical and
 431 subtropical biomes. Different superscript letters indicate significant ($p < 0.05$) Tukey tests
 432 of paired differences between biomes. Asterisks indicate statistically significant differences
 433 from zero for the paired differences between hydrometeorological couplings.

Biome	R^2_{VPD}	R^2_{SWC}	R^2_{PPFD}	R^2_{FULL}	$R^2_{VPD} - R^2_{SWC}$	$R^2_{VPD} - R^2_{PPFD}$	$R^2_{SWC} - R^2_{PPFD}$	Number of sites
DRY	0.31 A	0.183 A	0.189 A	0.389 A	0.127*** BC	0.121*** AB	-0.006 A	7
WOOD	0.436 B	0.412 B	0.281 AB	0.619 B	0.024 A	0.155*** B	0.131*** B	29
TEMP	0.461 B	0.389 B	0.358 C	0.544 B	0.072*** AB	0.103*** A	0.031* A	70
BOR	0.575 ABC	0.45 AB	0.481 BC	0.603 AB	0.124 ABC	0.093 AB	-0.031 AB	8
TROP	0.601 C	0.4 B	0.457 C	0.627 B	0.201*** C	0.144*** AB	-0.057. A	8

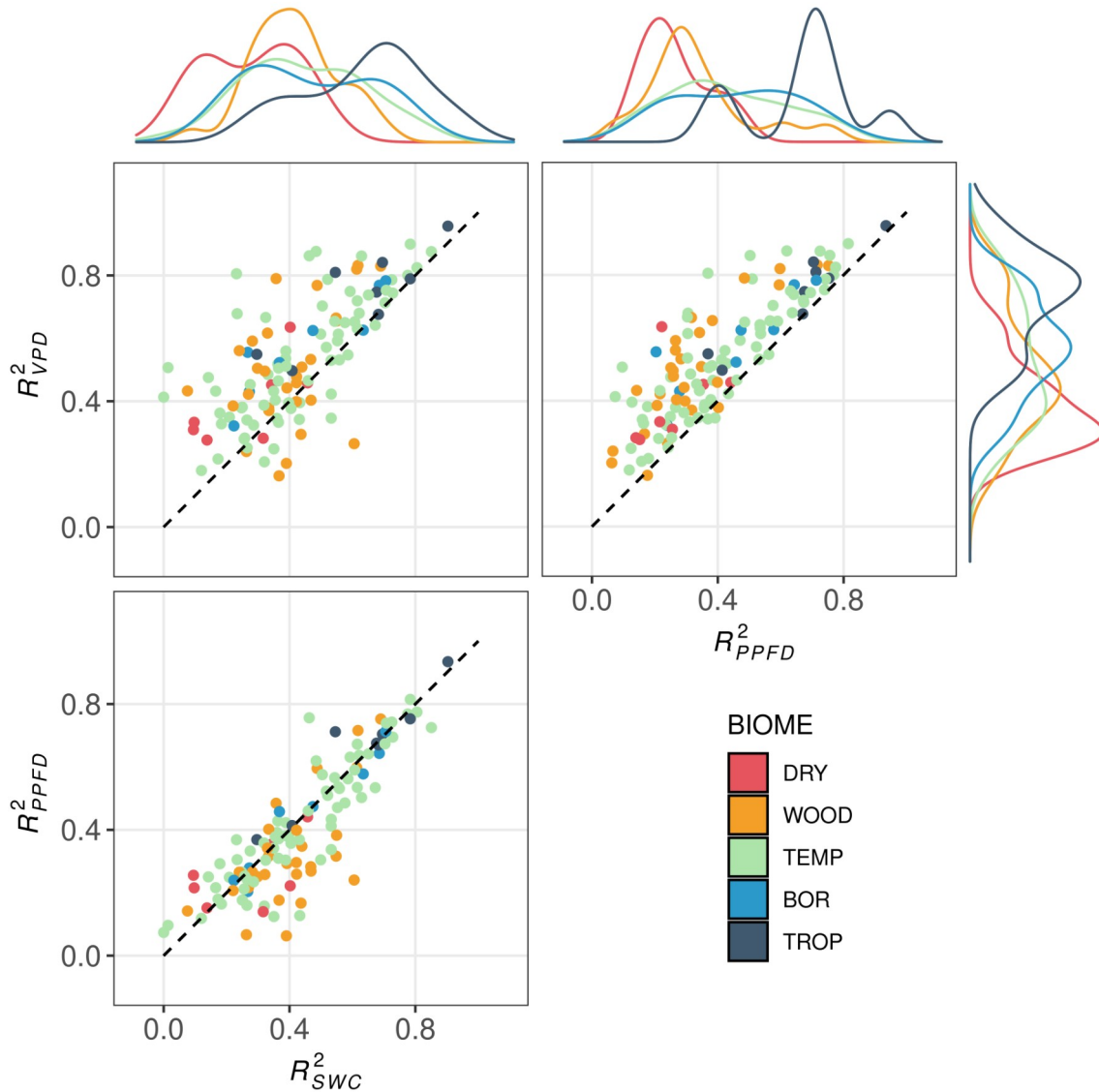
434 Statistical significant levels: "." $p < 0.1$; "*" $p < 0.05$; "***" $p < 0.01$; "****" $p < 0.001$

Table 2. Parameters of the models explaining G_{Asw} coupling to VPD, SWC, PPFD and to all three hydrometeorological drivers (R^2_{VPD} , R^2_{SWC} , R^2_{PPFD} and R^2_{FULL} , respectively) as a function of climatic, soil and stand structure variables. log(PPET): logarithm of precipitation over potential evapotranspiration [% $\log(\text{mm mm}^{-1})^{-1}$]; log(P-PETsd): logarithm of the standard deviation of the difference between precipitation and potential evapotranspiration [% $\log(\text{mm})^{-1}$]; Clay percentage [% $\%^{-1}\text{clay}$]; Total Nitrogen [% (Kg $\text{g}^{-1})^{-1}$]; Bedrock depth [% cm^{-1}]; Stand Height [% m^{-1}]; LAI: leaf area index [% ($\text{m}^2 \text{m}^{-2})^{-1}$]. NI means that the variable was not included in the model after model selection. The R^2 of each multiple regression is also shown.

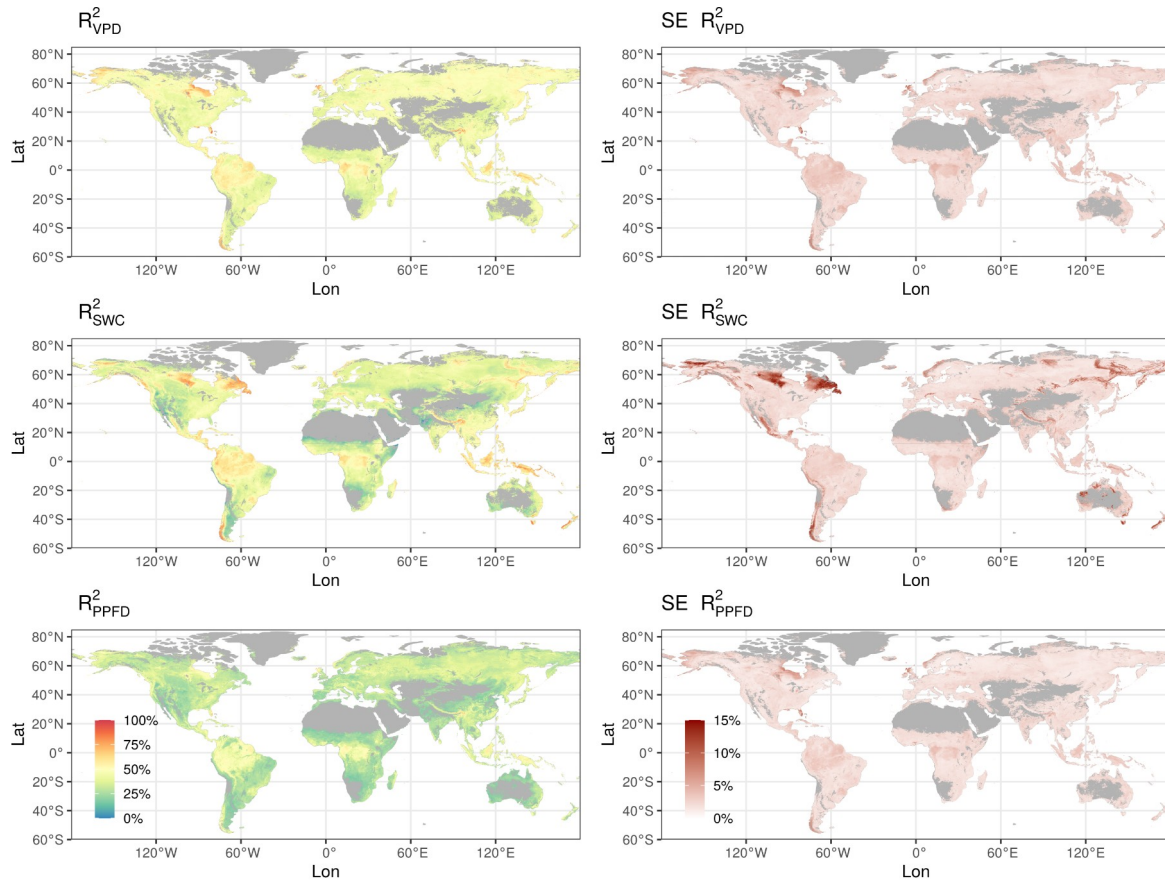
Variable	Intercept [%]	Climate		Soil			Vegetation structure		
		log(PPET)	log(P-PETsd)	Clay	Total Nitrogen	Bedrock depth	Stand Height	LAI	R^2
R^2_{VPD}	25.927 ***	NI	NI	0.314 ***	3.522 ***	NA	0.746 ***	-1.524 .	0.297
R^2_{SWC}	61.591 ***	11.692 ***	NI	0.475 ***	NI	-0.174 *	0.429 ***	-1.206 ns	0.521
R^2_{PPFD}	10.741 ***	NI	NI	0.230**	2.873 ***	NI	0.762 ***	NI	0.365
R^2_{FULL}	80.342 ***	5.932 *	NI	0.470***	1.849 *	-0.198 *	0.595 ***	-1.961 *	0.351

435

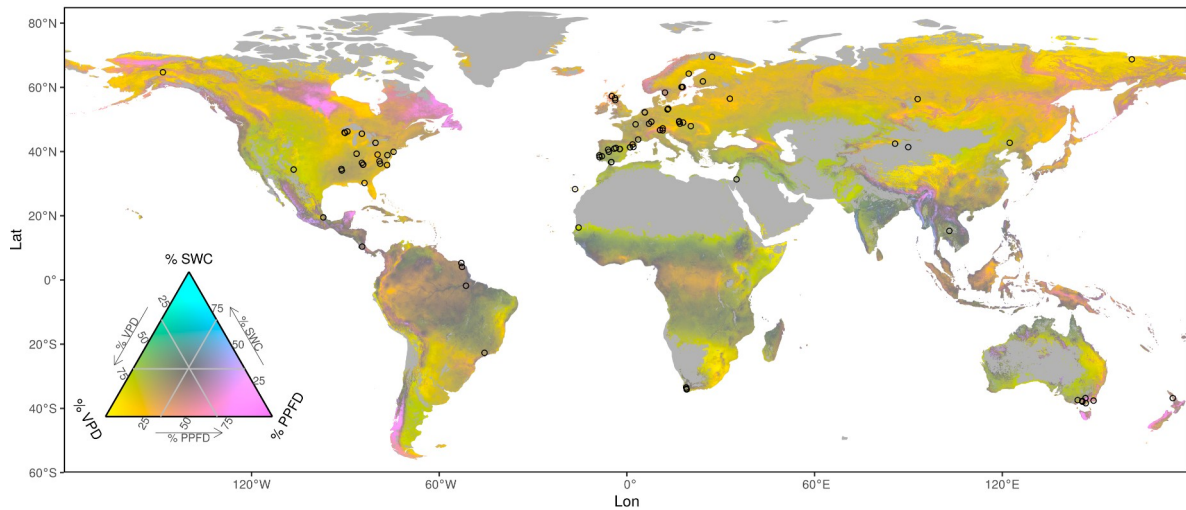
Statistical significant levels: "." $p < 0.1$; "*" $p < 0.05$; "***" $p < 0.01$; "****" $p < 0.001$; ns not significant.



436 Figure 1. Bi-variate and uni-variate distributions of the coupling of G_{Asw} to the
 437 hydrometeorological drivers studied: vapour pressure deficit (R^2_{VPD}), soil water content
 438 (R^2_{SWC}) and radiation (R^2_{PPFD}) for different biomes. Points correspond to site-level modelled
 439 conditional R^2 values. Colours represent different biomes, DRY: dry and desert biomes;
 440 WOOD: woodlands and shrublands; TEMP: temperate biomes; BOR: boreal and tundra;
 441 TROP: tropical and subtropical biomes. Dashed black line shows 1:1 relation.



443 Figure 2. Global projection of $G_{A_{sw}}$ coupling to VPD, SWC and PPF (R^2_{VPD} , R^2_{SWC} and
 444 R^2_{PPFD} , respectively), obtained from regression models of each coupling as a function of
 445 climatic, soil and stand structure variables (left panels). Right panels show projected
 446 Standard Error of the corresponding model.



447 Figure 3. Relative importance (partial R^2) of the three hydrometeorological drivers of
 448 transpiration regulation calculated from the complete (FULL) model, and projected at the
 449 global scale using linear models with climate, soil and vegetation structural variables as
 450 explanatory variables. Grid values were calculated using the ‘tricolore’ package (Schöley &
 451 Kashnitsky, 2020) for each cell as the relative value of the projections of the relative
 452 importance of each hydrometeorological variable. Colour gradient indicate the relative
 453 importance of the three hydrometeorological constraints. Light grey colour are deserts or
 454 non-forested areas. % VPD: vapour pressure deficit relative importance. % SWC: soil water
 455 content relative importance. % PPF: photosynthetic photon flux density relative
 456 importance. Points indicate locations of study sites.

457

Vapour pressure deficit is the main driver of tree canopy conductance across biomes

Víctor Flo¹, Jordi Martínez-Vilalta^{1,2}, Víctor Granda¹, Maurizio Mencuccini^{1,3}, Rafael Poyatos^{1,2}

¹CREAF, E08193 Bellaterra (Cerdanyola del Vallès), Catalonia, Spain

²Univ Autònoma de Barcelona, Cerdanyola del Vallès 08193, Spain

³ICREA, Barcelona 08010, Spain

Contents of this file

Figures S1 to S8

Tables S1 to S4

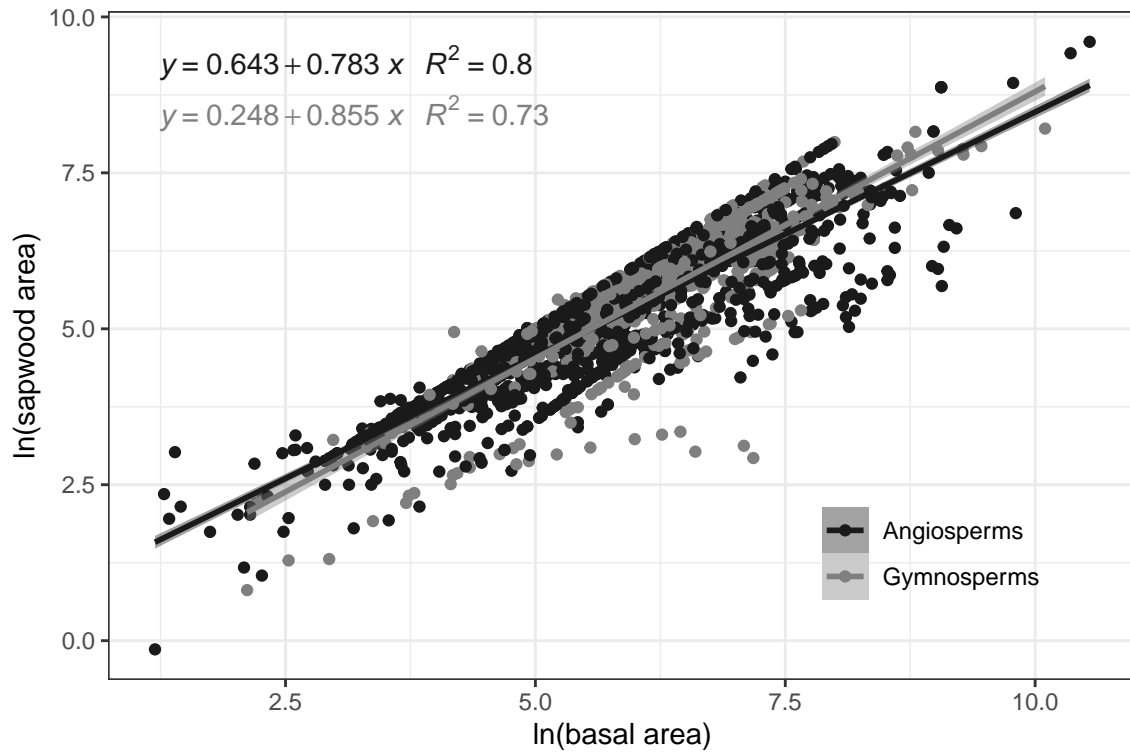


Figure S1: SAPFLUXNET global scaling relationship between basal area and sapwood area. Basal area and sapwood area are both in cm². Shaded areas are 95% model confidence interval.

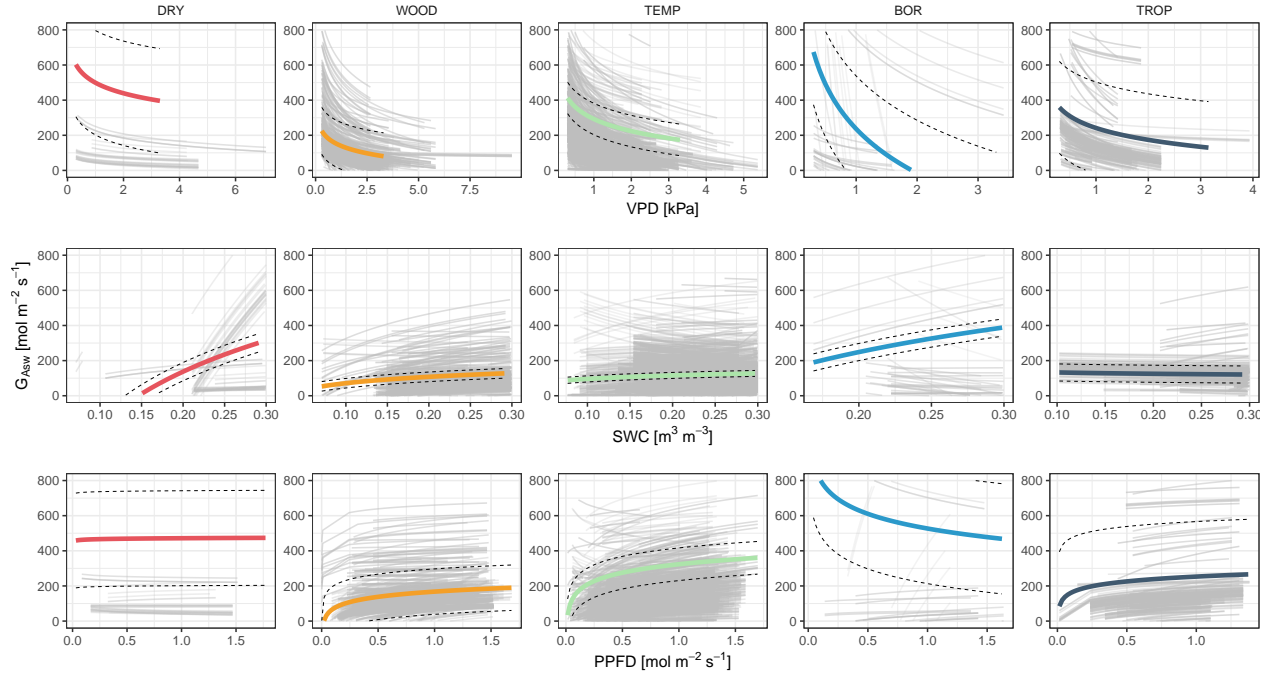


Figure S2: Log relationships of the three environmental variables estimated with the FULL model (VPD + SWC + PPF) and grouped by biome. Coloured lines are biome-averaged models calculated from LMM predictions with G_{Asw} as response variable and the neperian logarithm of the environmental constrains as explanatory variables. Dashed line shows standard error of the average models calculated with bootstrap prediction using 100 simulations.

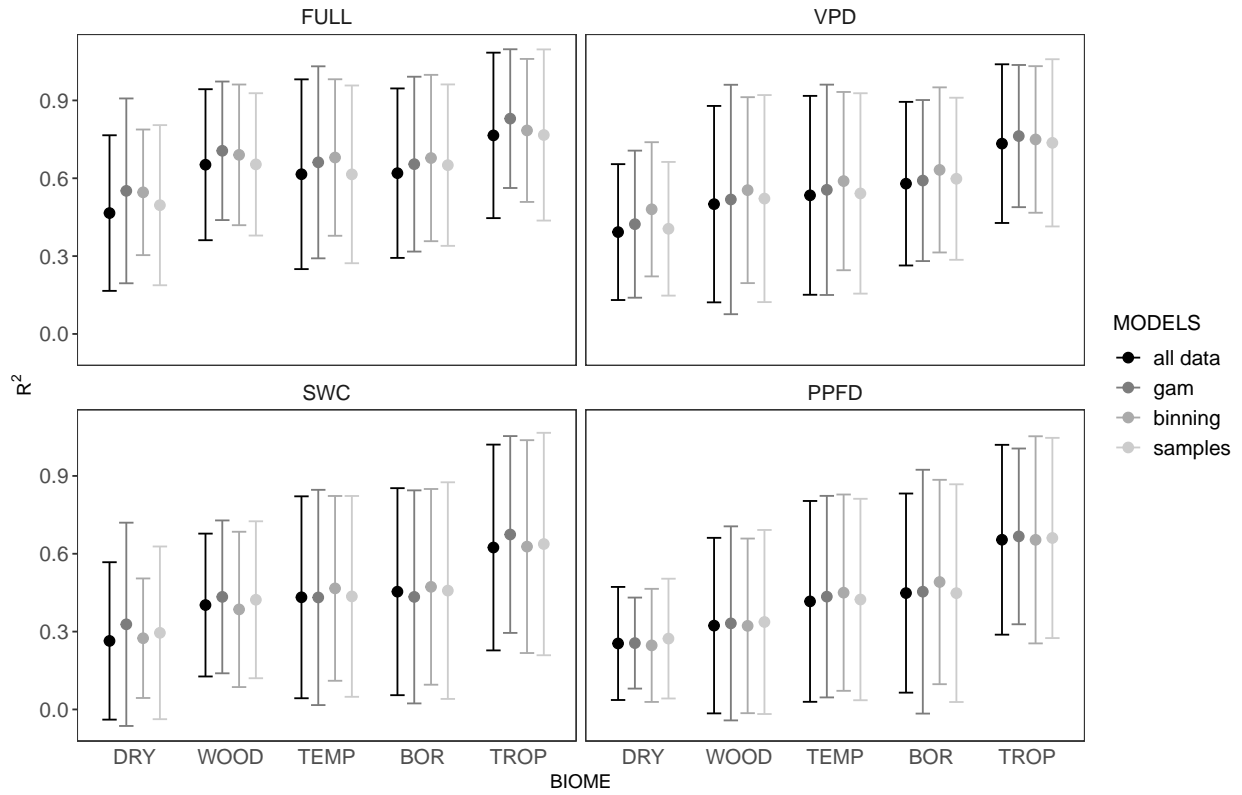


Figure S3: Comparison of biomes R_{FULL}^2 (VPD + SWC + PPFD), R_{VPD}^2 (VPD), R_{SWC}^2 (SWC) and R_{PPFD}^2 (PPFD) calculated with the four modelling approaches: using linear mixed models on all data, binned data and sampled data and, using GAM models on all data. Dots are mean values for each biome and error bars represent two standard deviations. There were no intra-biome significant differences among models.

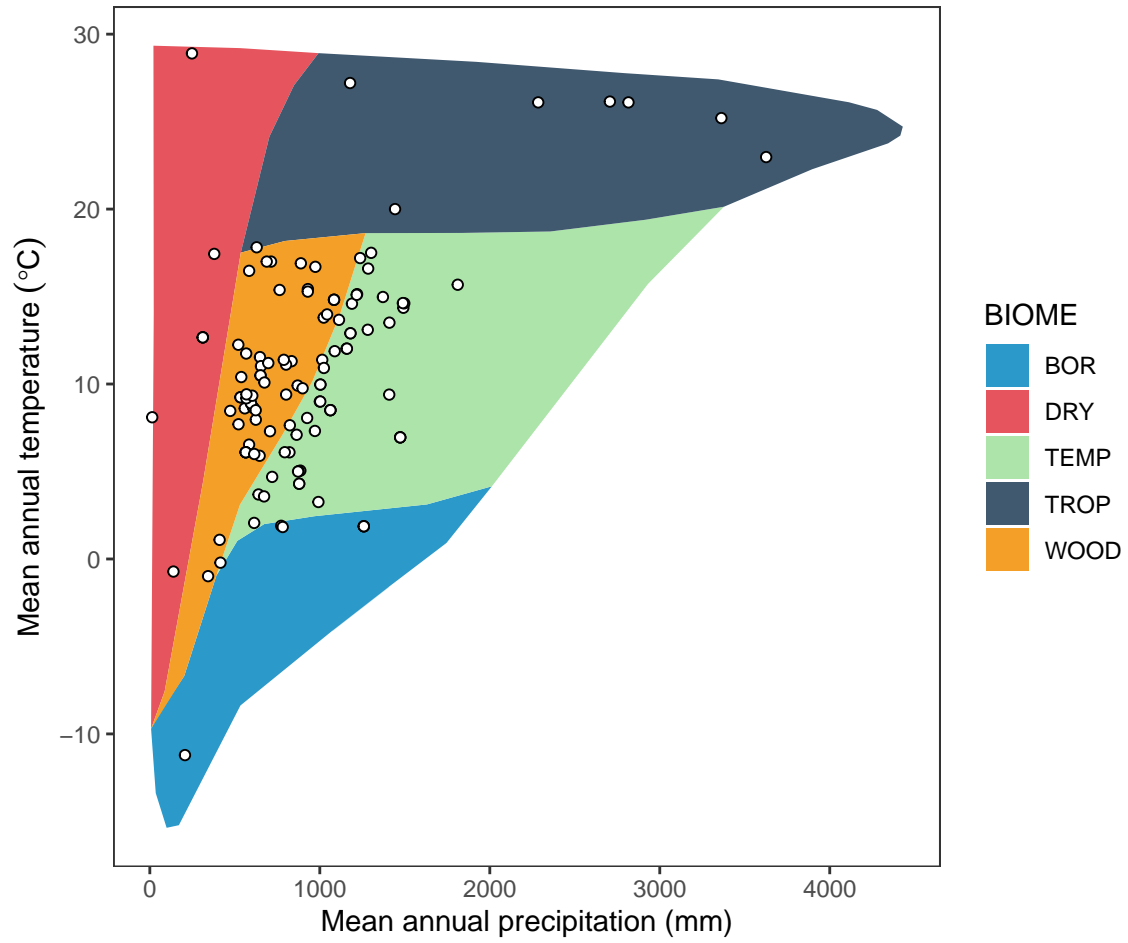


Figure S4: Bioclimatic distribution of the SAPFLUXNET datasets used in the study. Points show the different datasets in a Whittaker diagram showing the classification of the aggregated biomes used in the study.

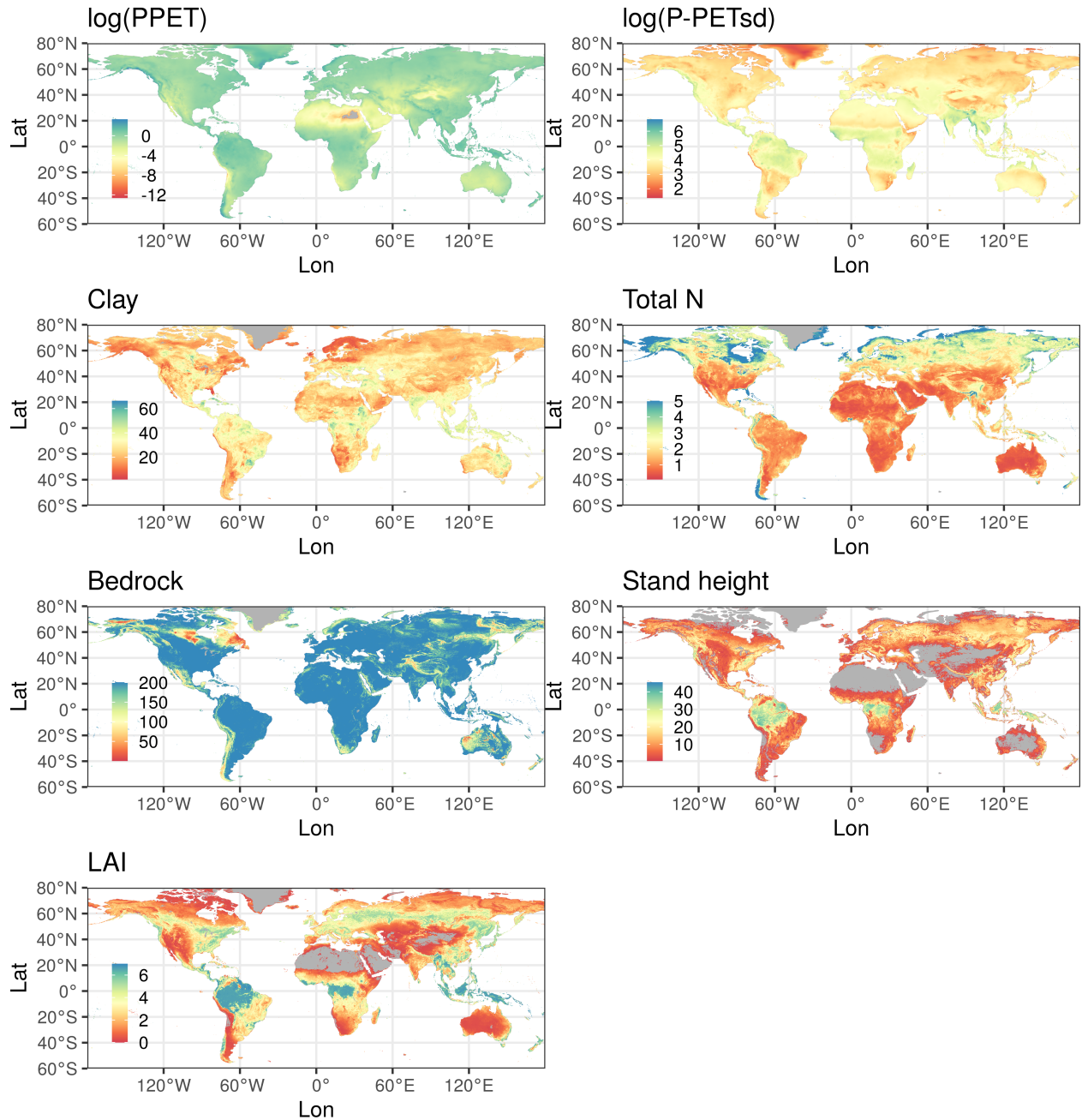


Figure S5: Global projection of climatic, soil and stand structure variables. $\log(\text{PPET})$: logarithm of precipitation over potential evapotranspiration [$\log(\text{mm mm}^{-1})$]; $\log(\text{P-PET}_{\text{sd}})$: logarithm of the standard deviation of the difference between precipitation and potential evapotranspiration [$\log(\text{mm})$]; Clay: percentage of clay in the soil; Total N: total nitrogen in the soil [g kg^{-1}]; Bedrock [cm]; Stand height [m]; LAI: leaf area index [$\text{m}^2 \text{m}^{-2}$]. Total N values above 5 g kg^{-1} were truncated.

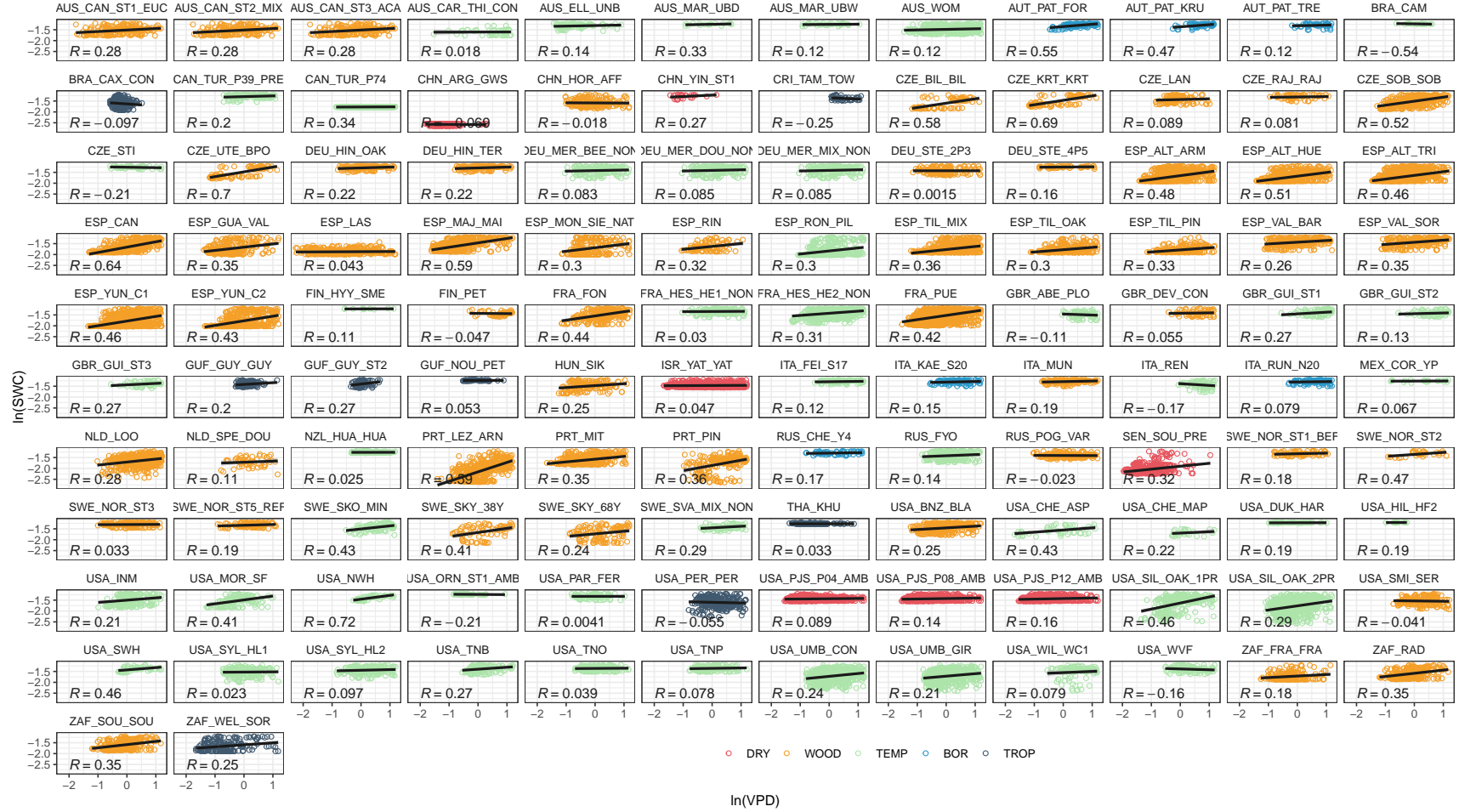


Figure S6: Correlations at the site level between VPD and SWC. R values are Pearson correlations. Different colors indicate the biome. DRY: dry and desert biomes; WOOD: woodlands and shrublands; TEMP: temperate biomes; BOR: boreal and tundra; TROP: tropical and subtropical biomes.

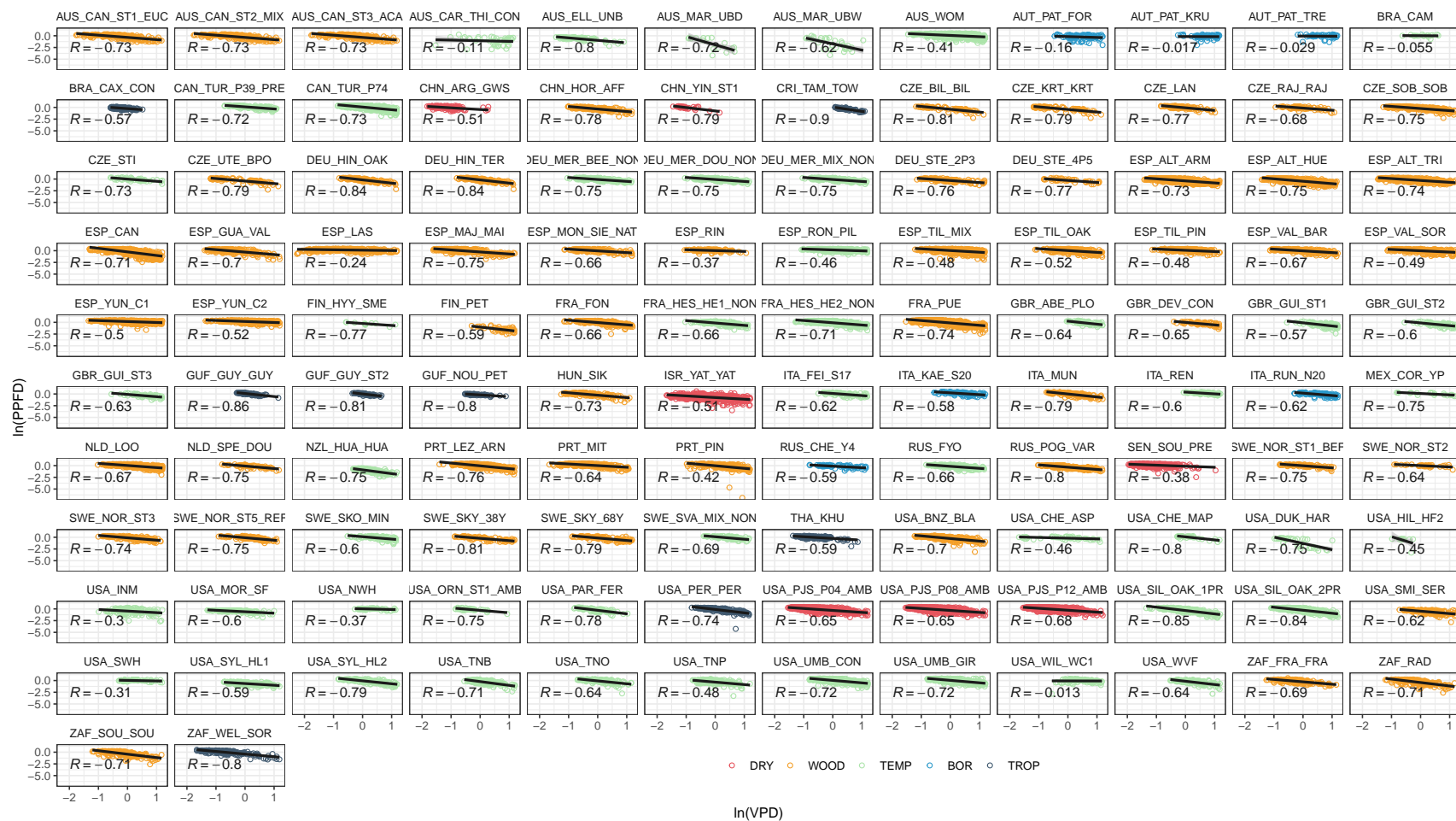


Figure S7: Correlations at the site level between VPD and PPFD. R values are Pearson correlations. Different colors indicate the biome. DRY: dry and desert biomes; WOOD: woodlands and shrublands; TEMP: temperate biomes; BOR: boreal and tundra; TROP: tropical and subtropical biomes.

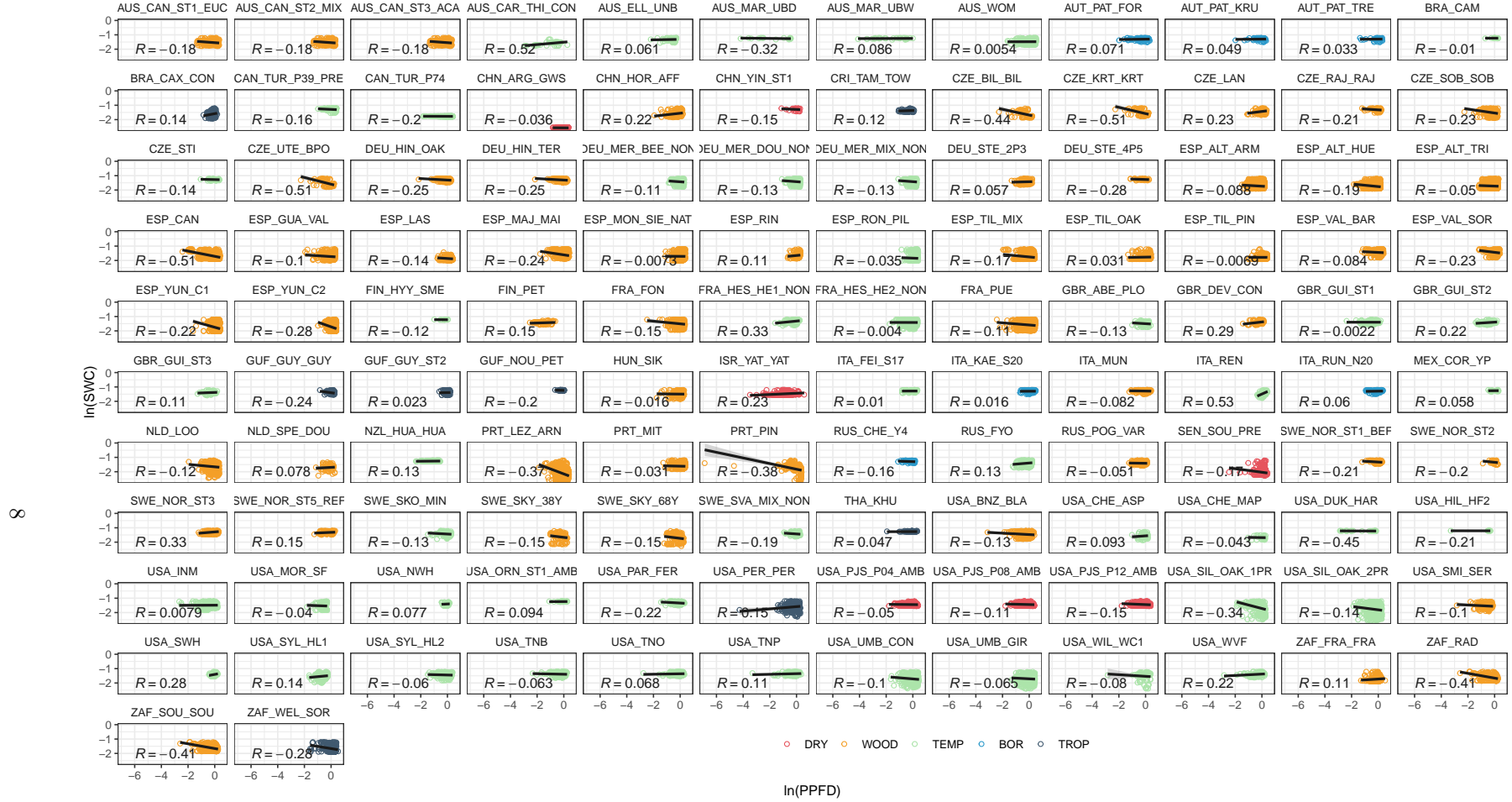


Figure S8: Correlations at the site level between PPF and SWC. R values are Pearson correlations. Different colors indicate the biome. DRY: dry and desert biomes; WOOD: woodlands and shrublands; TEMP: temperate biomes; BOR: boreal and tundra; TROP: tropical and subtropical biomes.

Table S1: SAPFLUXNET stand treatments included in the this study.

Plot treatment
NA
None
Control
control
Ambient Control
Control - Unthinned
natural conditions
Reference
1Premortality
2premortality
distructive sampling
Girdling early successional
Pre-thinning
Before thinning
Before Thinning
non thinned
none (periodict thinning every 5-6 years 20 to 25% of basal area)
Radiation Level
AMBIENT CO2 FACE rings
fertilization at plantation
AcaciaMonoculture
MixtureEucalyptusAndAcacia
EucalyptusMonoculture
Pre Irrigation

Table S2: SAPFLUXNET sites included in the study. Biome was estimated using a Whittaker diagram. *Indicates that the biome was manually adjusted and confirmed by SAPFLUXNET contributors.

Site code	Latitude	Longitude	Biome	# Tree-days	# Species	# Trees
AUS_CAN_ST1_EUC	-37.58	149.17	WOOD	500	1	12
AUS_CAN_ST2_MIX	-37.58	149.17	WOOD	1077	2	22
AUS_CAN_ST3_ACA	-37.58	149.17	WOOD	609	1	12
AUS_CAR_THI_CON	-38.38	146.68	TEMP	69	1	3
AUS_ELL_UNB	-36.78	146.58	TEMP	140	1	2
AUS_MAR_UBD	-37.69	145.56	TEMP	32	2	2
AUS_MAR_UBW	-37.89	145.57	TEMP	121	3	5
AUS_WOM	-37.42	144.09	TEMP	4454	2	11
AUT_PAT_FOR	47.21	11.45	BOR	286	1	3
AUT_PAT_KRU	47.21	11.45	BOR	105	1	2
AUT_PAT_TRE	47.21	11.45	BOR	133	1	3
BRA_CAM	-22.69	-45.52	TROP*	89	1	5
BRA_CAX_CON	-1.79	-51.43	TROP	2406	8	15
CAN_TUR_P39_PRE	42.71	-80.36	TEMP	2225	1	18
CAN_TUR_P74	42.71	-80.35	TEMP	10586	1	16
CHN_ARG_GWS	41.38	89.94	DRY	300	1	2
CHN_HOR_AFF	42.72	122.37	WOOD	2786	1	16
CHN_YIN_ST1	42.45	85.72	DRY	122	1	5
CRI_TAM_TOW	10.39	-84.63	TROP	1266	17	26
CZE_BIL_BIL	49.25	16.69	TEMP*	400	1	6
CZE_KRT_KRT	49.32	16.75	TEMP*	435	1	6
CZE_LAN	48.68	16.95	TEMP*	1775	3	17
CZE_RAJ_RAJ	49.44	16.70	TEMP*	360	1	6
CZE_SOB_SOB	49.25	16.69	TEMP*	1727	1	6
CZE_STI	49.04	17.97	TEMP	348	1	8
CZE_UTE_BPO	49.28	16.65	TEMP*	456	1	6
DEU_HIN_OAK	53.33	13.19	TEMP*	864	1	8
DEU_HIN_TER	53.33	13.19	TEMP*	1954	2	16
DEU_MER_BEE_NON	49.27	7.81	TEMP	841	1	8
DEU_MER_DOU_NON	49.27	7.81	TEMP	895	1	7
DEU_MER_MIX_NON	49.27	7.81	TEMP	1945	2	17
DEU_STE_2P3	53.10	13.00	TEMP*	1228	1	10
DEU_STE_4P5	53.10	13.00	TEMP*	402	1	10
ESP_ALT_ARM	40.78	-2.33	WOOD	8306	3	15
ESP_ALT_HUE	40.79	-2.29	WOOD	3698	2	8
ESP_ALT_TRI	40.80	-2.23	WOOD	5411	2	12
ESP_CAN	41.43	2.07	WOOD	6871	4	21
ESP_GUA_VAL	40.90	-4.03	WOOD	3424	1	24
ESP_LAS	28.31	-16.57	WOOD	4406	1	10
ESP_MAJ_MAI	39.94	-5.77	WOOD	2833	1	6
ESP_MON_SIE_NAT	41.12	-3.50	WOOD	2587	3	20
ESP_RIN	40.60	-6.02	WOOD	770	1	8
ESP_RON_PIL	36.69	-5.02	TEMP	4114	2	12
ESP_TIL_MIX	41.33	1.01	WOOD	15699	2	32
ESP_TIL_OAK	41.33	1.01	WOOD	2381	1	10
ESP_TIL_PIN	41.33	1.01	WOOD	1976	1	9
ESP_VAL_BAR	42.20	1.82	WOOD	1394	1	12
ESP_VAL_SOR	42.20	1.81	WOOD	1943	1	13
ESP_YUN_C1	36.72	-4.97	WOOD	2935	1	6
ESP_YUN_C2	36.72	-4.97	WOOD	830	1	6
FIN_HYY_SME	61.85	24.29	TEMP	10	1	1
FIN_PET	69.49	27.23	BOR*	216	1	7
FRA_FON	48.48	2.78	TEMP*	720	1	3
FRA_HES_HE1_NON	48.67	7.06	TEMP	1273	1	10
FRA_HES_HE2_NON	48.67	7.06	TEMP	4167	1	10
FRA_PUE	43.74	3.60	WOOD	23566	1	25
GBR_ABE_PLO	56.62	-3.80	TEMP	692	1	15
GBR_DEV_CON	56.03	-3.72	TEMP*	215	1	4
GBR_GUI_ST1	57.27	-4.82	TEMP	834	1	15

Table S2: SAPFLUXNET sites included in the study. Biome was estimated using a Whittaker diagram. *Indicates that the biome was manually adjusted and confirmed by SAPFLUXNET contributors. (continued)

Site code	Latitude	Longitude	Biome	# Tree-days	# Species	# Trees
GBR_GUI_ST2	57.27	-4.82	TEMP	621	1	9
GBR_GUI_ST3	57.27	-4.82	TEMP	444	1	8
GUF_GUY_GUY	5.28	-52.92	TROP	710	6	6
GUF_GUY_ST2	5.28	-52.91	TROP	885	7	11
GUF_NOU_PET	4.08	-52.68	TROP	923	10	22
HUN_SIK	47.93	20.44	WOOD	550	2	4
ISR_YAT_YAT	31.34	35.05	DRY	15766	1	24
ITA_FEI_S17	46.69	10.61	TEMP	378	1	6
ITA_KAE_S20	46.70	10.61	BOR	586	1	6
ITA_MUN	46.68	10.58	TEMP*	885	1	6
ITA_REN	46.59	11.43	TEMP	577	3	8
ITA_RUN_N20	46.70	10.64	BOR	766	2	8
MEX_COR_YP	19.49	-97.04	TEMP	113	1	7
NLD_LOO	52.17	5.74	TEMP*	3033	1	6
NLD_SPE_DOU	52.25	5.69	TEMP*	150	1	3
NZL_HUA_HUA	-36.80	174.49	TEMP	1107	1	6
PRT_LEZ_ARN	38.83	-8.82	WOOD	1764	1	4
PRT_MIT	38.54	-8.00	WOOD	1510	1	4
PRT_PIN	38.25	-8.76	WOOD	2991	2	20
RUS_CHE_Y4	68.74	161.41	BOR	587	1	11
RUS_FYO	56.46	32.92	TEMP	2338	3	17
RUS_POG_VAR	56.36	92.95	TEMP*	1290	3	9
SEN_SOU_PRE	16.34	-15.43	DRY	1706	1	3
SWE_NOR_ST1_BEF	60.09	17.48	TEMP*	843	2	22
SWE_NOR_ST2	60.09	17.48	TEMP*	194	2	6
SWE_NOR_ST3	60.09	17.48	TEMP*	1195	2	37
SWE_NOR_ST5_REF	60.08	17.48	TEMP*	1255	3	25
SWE_SKO_MIN	58.36	12.15	TEMP	1072	1	11
SWE_SKY_38Y	60.13	17.84	TEMP*	455	1	12
SWE_SKY_68Y	60.10	17.83	TEMP*	1046	2	12
SWE_SVA_MIX_NON	64.26	19.77	TEMP	1549	2	20
THA_KHU	15.27	103.08	TROP	1278	1	6
USA_BNZ_BLA	64.70	-148.32	BOR*	1705	1	6
USA_CHE_ASP	45.94	-90.27	TEMP	3995	6	142
USA_CHE_MAP	45.95	-90.26	TEMP	3378	2	145
USA_DUK_HAR	36.98	-79.09	TEMP	621	6	33
USA_HIL_HF2	36.22	-78.86	TEMP	263	5	22
USA_INM	39.32	-86.41	TEMP	1648	6	9
USA_MOR_SF	39.32	-86.41	TEMP	680	4	6
USA_NWH	34.58	-91.26	TEMP	525	2	10
USA_ORN_ST1_AMB	35.90	-84.33	TEMP	310	1	8
USA_PAR_FER	35.80	-76.67	TEMP	736	1	8
USA_PER_PER	30.21	-83.87	TROP	18180	1	80
USA_PJS_P04_AMB	34.39	-106.53	DRY	12129	2	10
USA_PJS_P08_AMB	34.39	-106.53	DRY	10754	2	10
USA_PJS_P12_AMB	34.39	-106.53	DRY	12528	2	10
USA_SIL_OAK_1PR	39.92	-74.60	TEMP	2304	4	18
USA_SIL_OAK_2PR	39.92	-74.60	TEMP	6790	4	22
USA_SMI_SER	38.89	-76.56	TEMP*	1733	5	30
USA_SWH	34.11	-91.13	TEMP	956	2	16
USA_SYL_HL1	46.24	-89.35	TEMP	8620	3	48
USA_SYL_HL2	46.24	-89.35	TEMP	3678	4	20
USA_TNB	36.47	-84.70	TEMP	1240	4	8
USA_TNO	35.97	-84.28	TEMP	1271	5	9
USA_TNP	35.96	-84.29	TEMP	1342	5	9
USA_UMB_CON	45.56	-84.71	TEMP	17923	5	57
USA_UMB_GIR	45.56	-84.70	TEMP	19175	4	57
USA_WIL_WC1	45.81	-90.09	TEMP	1306	5	16
USA_WVF	39.06	-79.69	TEMP	989	5	8

Table S2: SAPFLUXNET sites included in the study. Biome was estimated using a Whittaker diagram. *Indicates that the biome was manually adjusted and confirmed by SAPFLUXNET contributors. (*continued*)

Site code	Latitude	Longitude	Biome	# Tree-days	# Species	# Trees
ZAF_FRA_FRA	-33.88	19.06	WOOD	563	1	3
ZAF_RAD	-34.08	19.11	WOOD	660	1	3
ZAF_SOU_SOU	-34.09	19.09	WOOD	424	1	2
ZAF_WEL_SOR	-33.48	18.96	WOOD*	538	1	3

Table S3: Table of equivalence between Whittaker biomes and the groups of biomes used in the study.

Original biome name	Study biome group
Desert	DRY
Temperate grassland desert	DRY
Subtropical desert	DRY
Woodland/shrubland	WOOD
Temperate forest	TEMP
Boreal forest	BOR
Tundra	BOR
Tropical rainforest	TROP
Tropical seasonal forest/savanna	TROP

Table S4: Summary table of site level R_{VPD}^2 , R_{SWC}^2 , R_{PPFD}^2 , climate, soil properties and vegetation structure data. PPET is in [mm mm⁻¹], P-PET_{sd} is in [mm], Clay and Sand are in [%], Total N is in [g kg⁻¹], Stand height is in [m], LAI is in [m²_{leaves} m²_{soil}]. Letters show data source: a = SAPFLUXNET, b = Global rasters, c = SAPFLUXNET plant height.

Site code	R_{VPD}^2	R_{SWC}^2	R_{PPFD}^2	Relimp VPD	Relimp SWC	Relimp PPFD	PPET	P - PET _{sd}	Clay	Sand	Total N	Bedrock	Stand height	LAI
AUS_CAN_ST1_EUC	0.77	0.49	0.60	0.66	0.34	0.00	1.23	47.52	26.30 b	45.10 b	1.02	184	22.00 a	1.39 a
AUS_CAN_ST2_MIX	0.83	0.62	0.72	0.83	0.17	0.00	1.23	47.52	26.30 b	45.10 b	1.02	184	21.80 a	2.07 a
AUS_CAN_ST3_ACA	0.83	0.69	0.75	0.84	0.15	0.02	1.23	47.52	26.30 b	45.10 b	1.02	184	11.80 a	1.35 a
AUS_CAR_THI_CON	0.41	0.00	0.07	0.81	0.05	0.14	1.36	49.01	27.20 b	44.30 b	2.34	111	17.21 a	4.80 a
AUS_ELL_UNB	0.86	0.46	0.76	0.98	0.00	0.02	1.08	67.16	26.70 b	48.50 b	1.95	63	25.00 a	6.20 b
AUS_MAR_UBD	0.81	0.23	0.37	0.82	0.15	0.04	1.35	70.37	26.60 b	44.60 b	1.90	89	25.00 a	2.10 a
AUS_MAR_UBW	0.90	0.78	0.81	0.89	0.00	0.11	1.21	65.38	27.90 b	43.90 b	2.00	173	40.00 a	2.30 a
AUS_WOM	0.79	0.52	0.51	0.79	0.00	0.20	1.09	69.35	25.90 b	52.90 b	1.97	172	22.00 a	2.20 a
AUT_PAT_FOR	0.77	0.69	0.64	0.94	0.00	0.06	2.17	16.78	5.00 a	60.00 a	3.94	180	12.00 a	4.30 b
AUT_PAT_KRU	0.43	0.27	0.28	0.84	0.07	0.09	2.17	16.78	5.00 a	60.00 a	3.94	180	0.75 a	4.30 b
AUT_PAT_TRE	0.56	0.27	0.20	0.70	0.30	0.00	2.17	16.78	5.00 a	60.00 a	3.94	180	4.00 a	4.30 b
BRA_CAM	0.84	0.70	0.70	0.65	0.27	0.07	1.66	88.82	27.60 b	52.00 b	2.26	200	12.00 a	5.30 a
BRA_CAX_CON	0.75	0.68	0.68	0.73	0.00	0.27	1.90	122.90	8.00 a	79.00 a	1.45	197	38.00 b	5.30 a
CAN_TUR_P39_PRE	0.49	0.33	0.31	0.72	0.09	0.19	1.39	42.08	1.00 a	98.00 a	1.58	200	23.40 a	5.30 a
CAN_TUR_P74	0.21	0.32	0.16	0.31	0.33	0.35	1.39	41.87	1.00 a	98.00 a	1.60	200	16.20 a	6.70 a
CHN_ARG_GWS	0.45	0.34	0.35	0.52	0.45	0.03	0.01	63.51	17.70 b	46.00 b	0.70	172	7.90 a	0.36 a
CHN_HOR_AFF	0.37	0.33	0.32	0.51	0.47	0.01	0.59	31.24	8.00 a	83.00 a	1.00	200	9.05 a	1.61 a
CHN_YIN_ST1	0.46	0.46	0.44	0.48	0.41	0.11	0.19	35.09	20.80 b	32.90 b	2.41	148	10.60 a	0.50 b
CRI_TAM_TOW	0.68	0.68	0.67	0.47	0.15	0.37	3.57	159.99	36.10 b	34.70 b	2.75	200	30.60 a	3.30 a
CZE_BIL_BIL	0.53	0.53	0.41	0.52	0.20	0.29	0.71	28.98	29.60 b	27.40 b	1.91	200	14.00 a	6.00 b
CZE_KRT_KRT	0.61	0.50	0.30	0.62	0.04	0.34	0.85	27.00	26.00 b	27.40 b	2.10	200	17.00 a	5.70 b
CZE_LAN	0.74	0.73	0.69	0.67	0.07	0.26	0.66	37.49	17.80 a	71.80 a	2.46	200	36.00 a	6.04 a
CZE_RAJ_RAJ	0.35	0.36	0.39	0.37	0.03	0.60	0.99	26.14	21.80 b	33.90 b	1.96	200	18.00 a	4.60 b
CZE_SOB_SOB	0.40	0.43	0.13	0.49	0.30	0.21	0.71	28.98	29.60 b	27.40 b	1.91	200	21.00 a	6.00 b
CZE_STI	0.52	0.36	0.43	0.69	0.23	0.09	1.13	27.10	34.20 a	47.60 a	1.65	200	31.00 a	5.50 a
CZE_UTE_BPO	0.64	0.67	0.53	0.41	0.17	0.42	0.75	29.86	26.70 b	23.80 b	2.71	200	18.00 a	6.10 b
DEU_HIN_OAK	0.36	0.18	0.29	0.93	0.06	0.01	0.95	35.10	17.90 b	49.90 b	2.42	200	31.45 c	5.70 b
DEU_HIN_TER	0.22	0.17	0.18	0.74	0.02	0.24	0.95	35.10	18.00 b	50.50 b	2.05	200	24.42 c	5.60 b
DEU_MER_BEE_NON	0.38	0.25	0.27	0.80	0.05	0.15	1.48	47.33	4.00 a	71.00 a	2.56	200	23.00 a	5.90 a
DEU_MER_DOU_NON	0.38	0.25	0.18	0.58	0.29	0.14	1.48	47.33	4.00 a	71.00 a	2.56	200	29.00 a	5.30 a
DEU_MER_MIX_NON	0.35	0.21	0.25	0.85	0.01	0.14	1.48	47.33	4.00 a	71.00 a	2.56	200	30.00 a	6.10 a
DEU_STE_2P3	0.48	0.14	0.25	0.84	0.08	0.08	0.90	37.45	2.50 a	92.50 a	3.28	200	27.20 a	4.30 b
DEU_STE_4P5	0.45	0.28	0.33	0.64	0.32	0.04	0.90	37.45	2.50 a	92.50 a	3.28	200	27.20 a	4.30 b
ESP_ALT_ARM	0.44	0.39	0.29	0.77	0.19	0.04	0.66	65.80	21.90 b	41.50 b	1.27	187	19.00 b	1.09 a
ESP_ALT_HUE	0.42	0.27	0.22	0.77	0.00	0.23	0.51	63.08	21.60 b	35.90 b	1.46	200	8.64 c	1.50 b
ESP_ALT_TRI	0.48	0.42	0.26	0.67	0.21	0.13	0.57	63.48	21.00 b	40.00 b	1.31	196	4.89 a	1.60 b
ESP_CAN	0.51	0.44	0.35	0.62	0.09	0.28	0.94	46.91	32.90 b	28.30 b	1.76	179	10.80 a	3.30 a
ESP_GUA_VAL	0.50	0.30	0.25	0.71	0.00	0.29	0.68	69.09	24.80 b	40.90 b	1.27	200	12.00 a	3.80 a
ESP_LAS	0.24	0.26	0.07	0.43	0.45	0.13	1.63	37.89	1.00 a	70.00 a	1.65	197	10.30 a	3.60 a
ESP_MAJ_MAI	0.53	0.47	0.28	0.69	0.15	0.16	0.76	97.45	9.00 a	80.00 a	1.18	200	7.00 a	0.30 a
ESP_MON_SIE_NAT	0.38	0.33	0.40	0.49	0.05	0.45	0.62	63.05	20.80 b	41.90 b	1.45	200	22.00 a	3.30 b
ESP_RIN	0.82	0.61	0.60	0.96	0.00	0.04	0.85	76.30	15.00 a	9.00 a	2.17	200	7.40 a	3.40 a
ESP_RON_PIL	0.34	0.26	0.16	0.59	0.11	0.31	1.05	93.66	18.00 a	30.00 a	1.86	200	2.60 a	0.90 b
ESP_TIL_MIX	0.40	0.42	0.30	0.43	0.17	0.40	0.77	48.10	20.00 a	60.00 a	1.44	162	14.20 a	3.27 a
ESP_TIL_OAK	0.16	0.37	0.18	0.29	0.35	0.37	0.77	48.10	20.00 a	60.00 a	1.44	162	5.00 a	4.59 a
ESP_TIL_PIN	0.20	0.39	0.06	0.28	0.55	0.17	0.79	48.10	20.00 a	60.00 a	1.78	188	18.30 a	1.02 a

Table S4: Summary table of site level R_{VPD}^2 , R_{SWC}^2 , R_{PPFD}^2 , climate, soil properties and vegetation structure data. PPET is in [mm mm⁻¹], P-PET_{sd} is in [mm], Clay and Sand are in [%], Total N is in [g kg⁻¹], Stand height is in [m], LAI is in [m²_{leaves} m⁻²_{soil}]. Letters show data source: a = SAPFLUXNET, b = Global rasters, c = SAPFLUXNET plant height. (continued)

Site code	R_{VPD}^2	R_{SWC}^2	R_{PPFD}^2	Relimp VPD	Relimp SWC	Relimp PPFD	PPET	P - PET _{sd}	Clay	Sand	Total N	Bedrock	Stand height	LAI
ESP_VAL_BAR	0.56	0.24	0.27	0.87	0.00	0.13	0.70	34.07	32.63 a	9.81 a	1.94	200	10.60 a	2.10 a
ESP_VAL_SOR	0.50	0.32	0.26	0.66	0.10	0.24	0.78	32.15	20.00 a	60.00 a	2.04	200	11.00 a	2.40 a
ESP_YUN_C1	0.29	0.44	0.17	0.17	0.67	0.16	0.83	93.65	29.00 a	22.00 a	1.37	197	10.60 a	2.20 b
ESP_YUN_C2	0.27	0.61	0.24	0.22	0.43	0.35	0.78	91.33	29.00 a	22.00 a	1.37	188	11.60 a	2.50 b
FIN_HYY_SME	0.51	0.01	0.10	0.61	0.10	0.29	1.20	38.32	6.50 a	37.00 a	1.67	200	18.00 a	1.30 a
FIN_PET	0.63	0.63	0.58	0.40	0.60	0.01	1.13	26.34	7.30 b	60.80 b	5.08	200	3.76 a	0.61 a
FRA_FON	0.68	0.62	0.64	0.72	0.22	0.06	0.89	45.10	19.00 a	37.00 a	1.26	200	28.00 a	6.00 a
FRA_HES_HE1_NON	0.42	0.53	0.43	0.41	0.26	0.33	1.31	47.72	25.00 a	8.00 a	1.41	200	12.80 a	6.00 a
FRA_HES_HE2_NON	0.25	0.35	0.12	0.45	0.27	0.28	1.31	47.72	25.00 a	8.00 a	1.41	200	13.00 a	6.00 a
FRA_PUE	0.40	0.47	0.27	0.46	0.27	0.27	1.27	70.16	39.00 a	26.00 a	1.69	195	5.00 a	2.40 a
GBR_ABE_PLO	0.28	0.26	0.21	0.51	0.23	0.25	1.92	47.48	10.00 a	60.00 a	3.70	179	10.00 a	6.00 a
GBR_DEV_CON	0.88	0.48	0.62	0.93	0.04	0.04	1.43	44.38	14.80 b	56.90 b	3.44	200	15.00 a	1.92 a
GBR_GUI_ST1	0.80	0.78	0.77	0.58	0.01	0.41	3.19	68.11	3.70 b	80.40 b	14.26	197	11.00 a	0.92 a
GBR_GUI_ST2	0.59	0.55	0.47	0.59	0.06	0.35	3.19	68.11	3.70 b	80.40 b	14.26	197	13.30 a	0.94 a
GBR_GUI_ST3	0.82	0.81	0.77	0.66	0.03	0.31	3.19	68.11	3.70 b	80.40 b	14.26	197	14.30 a	1.57 a
GUF_GUY_GUY	0.96	0.90	0.93	0.82	0.07	0.11	2.88	135.18	43.00 a	48.00 a	1.53	200	35.00 a	7.00 a
GUF_GUY_ST2	0.79	0.78	0.75	0.46	0.49	0.04	3.02	141.34	43.20 a	47.80 a	1.66	200	35.00 a	6.70 a
GUF_NOU_PET	0.81	0.55	0.71	1.00	0.00	0.00	2.69	158.16	59.20 a	33.20 a	2.22	200	35.00 a	5.50 a
HUN_SIK	0.79	0.36	0.48	0.93	0.01	0.06	0.70	39.64	30.40 b	44.00 b	1.64	200	20.00 a	7.00 a
ISR_YAT_YAT	0.28	0.32	0.14	0.43	0.57	0.00	0.28	83.43	28.00 a	31.00 a	0.71	178	11.00 a	1.70 a
ITA_FEL_S17	0.54	0.39	0.30	0.68	0.13	0.19	1.08	22.97	8.00 a	76.00 a	3.11	117	20.00 a	3.10 b
ITA_KAE_S20	0.62	0.47	0.47	0.72	0.06	0.22	1.24	22.97	17.00 a	50.00 a	3.64	121	14.00 a	2.60 b
ITA_MUN	0.56	0.39	0.42	0.74	0.22	0.04	0.80	29.87	7.00 a	55.00 a	1.93	188	18.00 a	2.20 b
ITA_REN	0.79	0.73	0.74	0.99	0.00	0.01	1.61	12.59	17.70 b	47.90 b	2.73	143	27.00 b	4.60 b
ITA_RUN_N20	0.78	0.71	0.71	0.88	0.00	0.12	1.39	15.28	14.00 a	54.00 a	3.33	123	18.70 a	5.70 b
MEX_COR_YP	0.68	0.23	0.31	0.79	0.05	0.16	1.42	81.77	22.20 b	46.40 b	2.94	200	7.00 a	5.20 a
NLD_LOO	0.18	0.12	0.12	0.79	0.00	0.21	1.33	41.67	1.00 a	99.00 a	2.61	200	18.00 a	2.20 a
NLD_SPE_DOU	0.75	0.59	0.63	0.85	0.03	0.12	1.42	39.80	4.80 b	80.70 b	1.62	200	30.00 a	4.50 a
NZL_HUA_HUA	0.65	0.61	0.59	0.70	0.15	0.15	2.62	42.52	71.20 a	13.20 a	1.73	200	27.00 a	6.60 b
PRT_LEZ_ARN	0.59	0.28	0.27	0.78	0.01	0.21	0.72	77.42	5.04 a	90.38 a	1.52	200	12.00 a	1.50 a
PRT_MIT	0.66	0.55	0.32	0.61	0.33	0.06	0.51	80.80	16.10 b	64.50 b	1.33	200	7.50 a	0.55 a
PRT_PIN	0.65	0.55	0.38	0.65	0.32	0.02	0.76	74.76	16.60 b	61.20 b	1.26	200	12.60 a	1.10 b
RUS_CHE_Y4	0.32	0.22	0.24	0.94	0.00	0.06	0.62	34.23	21.10 b	23.20 b	4.96	200	7.00 a	1.30 b
RUS_FYO	0.61	0.56	0.54	0.81	0.02	0.17	1.24	30.87	18.20 b	48.80 b	3.77	198	23.50 a	3.50 a
RUS_POG_VAR	0.70	0.50	0.58	0.81	0.00	0.19	0.70	33.02	28.60 b	37.50 b	2.64	200	22.00 a	2.80 b
SEN_SOU_PRE	0.64	0.40	0.22	0.66	0.34	0.01	0.13	43.94	6.00 a	90.00 a	0.23	200	7.00 a	0.22 a
SWE_NOR_ST1_BEF	0.74	0.65	0.64	0.61	0.28	0.10	1.07	36.70	5.80 a	58.60 a	2.63	185	28.70 a	4.18 a
SWE_NOR_ST2	0.32	0.29	0.23	0.55	0.02	0.44	1.07	36.70	5.80 a	58.60 a	2.63	185	27.70 a	6.15 a
SWE_NOR_ST3	0.55	0.59	0.56	0.48	0.22	0.30	1.07	36.70	5.80 a	58.60 a	2.63	185	27.20 a	4.55 a
SWE_NOR_ST5_REF	0.53	0.56	0.53	0.48	0.20	0.32	1.07	36.55	19.20 b	43.50 b	2.83	190	20.00 a	5.00 a
SWE_SKO_MIN	0.71	0.70	0.67	0.52	0.04	0.44	1.60	45.86	17.30 b	52.00 b	2.48	133	28.00 a	6.50 a
SWE_SKY_38Y	0.34	0.43	0.37	0.05	0.94	0.00	1.39	33.61	21.70 b	43.80 b	3.93	184	13.60 a	3.98 a
SWE_SKY_68Y	0.35	0.53	0.34	0.05	0.83	0.11	1.30	33.80	18.90 b	46.50 b	4.15	184	20.30 a	3.83 a
SWE_SVA_MIX_NON	0.65	0.54	0.57	0.78	0.22	0.00	1.33	34.34	0.50 a	92.50 a	1.67	200	15.00 a	3.80 b
THA_KHU	0.50	0.41	0.41	0.78	0.21	0.01	0.83	84.24	10.00 a	65.00 a	0.75	200	15.00 a	3.90 a
USA_BNZ_BLA	0.52	0.37	0.46	0.68	0.21	0.10	0.69	33.86	10.30 b	36.80 b	2.57	200	3.00 a	3.60 b
USA_CHE_ASP	0.67	0.32	0.30	0.91	0.03	0.06	1.23	20.06	12.00 a	74.00 a	1.52	200	10.00 a	4.50 a

Table S4: Summary table of site level R_{VPD}^2 , R_{SWC}^2 , R_{PPFD}^2 , climate, soil properties and vegetation structure data. PPET is in [mm mm⁻¹], P-PET_{sd} is in [mm], Clay and Sand are in [%], Total N is in [g kg⁻¹], Stand height is in [m], LAI is in [m²_{leaves} m²_{soil}]. Letters show data source: a = SAPFLUXNET, b = Global rasters, c = SAPFLUXNET plant height. (continued)

Site code	R_{VPD}^2	R_{SWC}^2	R_{PPFD}^2	Relimp VPD	Relimp SWC	Relimp PPFD	PPET	P - PET _{sd}	Clay	Sand	Total N	Bedrock	Stand height	LAI
USA_CHE_MAP	0.57	0.52	0.52	0.76	0.06	0.18	1.22	19.85	6.63 a	59.31 a	2.54	200	18.00 a	3.90 a
USA_DUK_HAR	0.72	0.62	0.67	0.91	0.02	0.07	1.12	41.33	33.90 b	31.00 b	0.76	200	25.00 a	7.03 a
USA_HIL_HF2	0.75	0.71	0.74	0.61	0.00	0.39	1.14	37.46	26.00 a	43.00 a	0.71	200	15.00 a	5.50 a
USA_INM	0.40	0.35	0.38	0.56	0.00	0.44	1.18	39.20	26.70 b	8.00 b	1.05	200	30.00 a	4.90 a
USA_MOR_SF	0.65	0.58	0.49	0.90	0.09	0.01	1.18	39.20	30.00 a	10.00 a	1.05	200	27.00 a	5.00 a
USA_NWH	0.88	0.85	0.73	0.80	0.04	0.15	1.05	59.56	36.70 b	4.90 b	0.80	200	22.70 a	5.60 b
USA_ORN_ST1_AMB	0.63	0.62	0.53	0.51	0.10	0.39	1.14	61.36	24.00 a	21.00 a	0.85	200	17.90 a	5.50 a
USA_PAR_FER	0.43	0.17	0.22	0.69	0.04	0.27	1.32	25.96	10.00 a	60.00 a	1.75	200	18.00 a	4.20 a
USA_PER_PER	0.55	0.30	0.37	0.85	0.01	0.14	1.32	34.41	3.40 b	89.20 b	6.13	200	12.00 a	4.10 a
USA_PJS_P04_AMB	0.31	0.09	0.26	0.74	0.03	0.23	0.25	49.32	6.00 a	52.00 a	0.82	186	4.20 a	0.71 a
USA_PJS_P08_AMB	0.33	0.10	0.22	0.94	0.03	0.03	0.25	49.32	3.00 a	49.00 a	0.82	186	4.10 a	0.90 a
USA_PJS_P12_AMB	0.28	0.14	0.15	0.63	0.37	0.00	0.25	49.32	6.00 a	54.00 a	0.82	186	4.00 a	0.72 a
USA_SIL_OAK_1PR	0.38	0.40	0.36	0.29	0.58	0.13	1.36	38.70	1.00 a	98.00 a	0.74	200	9.50 a	3.60 a
USA_SIL_OAK_2PR	0.39	0.32	0.36	0.92	0.06	0.01	1.36	38.70	1.00 a	98.00 a	0.74	200	9.50 a	3.60 a
USA_SML_SER	0.51	0.37	0.37	0.67	0.32	0.01	1.03	40.05	28.70 b	30.90 b	0.82	200	40.00 a	5.80 b
USA_SWH	0.86	0.63	0.50	0.94	0.01	0.05	1.09	62.29	43.10 b	6.30 b	0.69	200	24.20 a	4.00 b
USA_SYL_HL1	0.46	0.36	0.38	0.97	0.03	0.00	1.27	25.01	8.90 b	51.00 b	1.41	200	27.00 a	5.40 b
USA_SYL_HL2	0.47	0.46	0.46	0.55	0.01	0.44	1.27	25.01	8.90 b	51.00 b	1.41	200	27.00 a	5.40 b
USA_TNB	0.25	0.27	0.24	0.41	0.12	0.46	1.39	48.33	21.60 b	34.90 b	0.84	200	25.00 a	4.70 a
USA_TNO	0.40	0.40	0.38	0.50	0.22	0.28	1.41	60.02	29.60 b	30.20 b	0.83	200	30.00 a	6.60 a
USA_TNP	0.33	0.36	0.31	0.40	0.37	0.23	1.41	61.60	31.60 b	26.60 b	0.81	200	25.00 a	4.50 a
USA_UMB_CON	0.51	0.39	0.38	0.79	0.03	0.18	1.30	30.60	1.00 a	92.00 a	2.02	200	29.00 a	3.50 a
USA_UMB_GIR	0.43	0.35	0.34	0.78	0.05	0.17	1.25	30.69	1.00 a	92.00 a	2.49	200	29.00 a	3.50 a
USA_WIL_WC1	0.33	0.18	0.16	0.82	0.16	0.02	1.19	20.23	6.90 b	53.20 b	1.01	200	24.30 a	6.20 b
USA_WVF	0.28	0.26	0.25	0.59	0.06	0.36	1.63	30.35	24.90 b	29.90 b	1.37	200	30.00 a	6.90 a
ZAF_FRA_FRA	0.43	0.08	0.14	0.92	0.00	0.08	0.90	99.17	20.00 b	69.90 b	0.95	200	20.00 a	1.80 a
ZAF_RAD	0.46	0.42	0.40	0.57	0.10	0.33	0.95	82.73	21.30 b	61.40 b	1.18	200	3.50 a	2.70 a
ZAF_SOU_SOU	0.39	0.22	0.21	0.59	0.06	0.35	0.97	86.39	23.00 b	61.90 b	1.13	200	4.00 a	3.00 a
ZAF_WEL_SOR	0.62	0.33	0.34	0.63	0.08	0.29	0.50	79.71	20.00 a	60.00 a	0.81	179	25.00 a	1.80 a